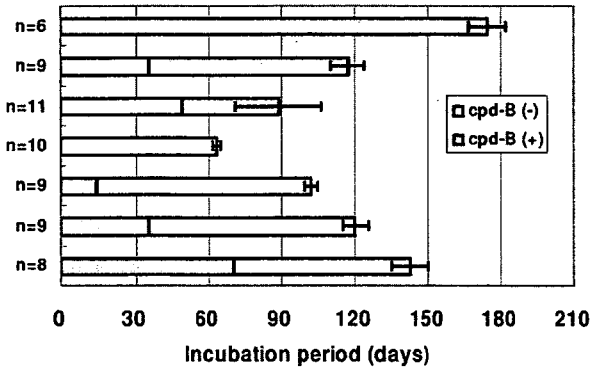

FIG. 3. cpd-B effects throughout various timings and durations of oral administration. Tga20 mice cerebrally infected with RML prion were treated with 0.2% cpd-B feed at different times and for different durations, and the incubation periods were assayed. Open bars indicate the durations of no treatment [cpd-B (−)]. Shaded bars indicate the durations of oral cpd-B treatment [cpd-B (+)].

treated hamsters (Fig. 2F). These results indicate that oral cpd-B treatment is not as effective for 263K prion.

Timing and duration of dosing. The effectiveness of cpd-B at various timings and durations of oral administration was analyzed in Tga20 mice that had been cerebrally infected with RML prion (Fig. 3). The incubation periods of the nontreated mice were 63.0 ± 1.8 days, whereas the incubation periods of the mice treated with 0.2% cpd-B feed were inversely correlated with the postinfection durations to the commencement of cpd-B treatment ($r = -0.79$; $P < 0.01$): 174.5 ± 7.6 days when started at day 0 postinfection, 117.2 ± 7.0 days when started at day 35 postinfection, and 88.7 ± 17.3 days when started at day 49 postinfection. On the other hand, the incubation periods of the mice treated with 0.2% cpd-B feed were also correlated with the durations of cpd-B treatment which started immediately after cerebral infection ($r = 0.95$, $P < 0.01$): 102.1 ± 2.9 days when treated for 14 days from the infection, 120.2 ± 5.2 days when treated for 35 days from the infection, and 142.5 ± 7.8 days when treated for 70 days from the infection. In addition, when the cpd-B treatment was discontinued during early disease stages, the remaining incubation times were longer than that of the control mice.

Pathological evaluation. The PrPres content in the brains of cpd-B-treated mice was analyzed sequentially by immunoblotting and compared with that in the nontreated control mice (Fig. 4A). The PrPres signals in the nontreated mice were very strong at the terminal stage of disease (day 63 postinfection). In contrast, in the mice treated with 0.1% cpd-B feed from the start of infection, PrPres signals were faint at day 63 postinfection and distinct at the terminal stage of disease (day 108 postinfection). However, the PrPres signals at the terminal stage of disease did not reach the high level shown by the nontreated control mice at that stage. Comparison of the signal intensities of the diglycosylated PrPres form showed that 6- to 15-fold-diluted samples from the nontreated terminal mice exhibited signal intensities similar to those of undiluted or 2-fold-diluted samples from the 0.1% cpd-B-treated terminal mice (Fig. 4B). Similarly, in the mice treated with 0.2% cpd-B feed from the start of infection, PrPres signals gradually increased according to the time course after infection: no signals were detected at day 63 postinfection, distinct signals were detected at day 120, and similar or more distinct signals were detected at the terminal stage of infection (day 154 postinfection). The PrPres signal levels of the 0.2% cpd-B-treated mice at the terminal stage of disease were indistinguishable from those of the 0.1% cpd-treated mice at the terminal stage of disease.

The glycoform patterns of PrPres differed completely. As shown in Fig. 4B, when the samples were diluted and reassayed so that the signal intensities of diglycosylated PrPres forms were equalized as much as possible, the difference was much more distinct. The glycoform patterns in the nontreated mice, which were uniform in the analyzed samples, were predominantly monoglycosylated, whereas the glycoform patterns in the cpd-B-treated mice were not necessarily uniform but were always predominantly diglycosylated. This predominance of diglycosylated PrPres was also observed for 263K prion (Fig. 4C) but not for other prion strains used in this study (data not shown).

Modification in the pathology of the brains of cpd-B-treated mice was analyzed (Fig. 4D). For nontreated control mice with an incubation period of 63 days, the brain showed prominent pathological changes consisting of abnormal PrP deposition and glial cell reaction in the thalamus, although the brains of the mice treated with 0.2% cpd-B feed showed no such pathological changes at day 63 postinfection and milder levels of abnormal PrP deposition at the terminal stage of disease (day 154 postinfection). No difference was apparent in the pattern or distribution of abnormal PrP deposition in the brains between the nontreated mice and the cpd-B-treated mice.

Infectivity analysis. Infectivity levels are inversely correlated with incubation periods (24). Therefore, infectivity levels of the brains of the mice treated with 0.2% cpd-B feed were evaluated by assaying the incubation periods of animals that had been cerebrally inoculated with the brain homogenate (Table 2). The 10^2-fold-diluted brain homogenates from the cpd-B-treated mice at day 63 postinfection exhibited incubation periods similar to those of the 10^5-fold- or greater diluted brain homogenates from the nontreated mice; the 10^2-fold-diluted brain homogenates from the cpd-B-treated mice at the terminal stage of disease (day 154 postinfection) showed incubation periods similar to those of the 10^4-fold- or 10^5-fold-diluted brain homogenates from the nontreated mice. The data indicate that the brains of mice treated with 0.2% cpd-B feed had much lower infectivity levels than those of the nontreated mice at the same time point after infection and even at the terminal stage of disease. A 100-fold to 1,000-fold difference in infectivity levels was apparent between the nontreated terminal mice and the cpd-B-treated terminal mice, although a less-than-100-fold difference in PrPres levels between the two mouse groups was estimated from the immunoblot data shown in Fig. 4B. On the other hand, no inconsistency was apparent in the gaps in the infectivity levels and the PrPres levels between the cpd-B-treated mice at day 63 postinfection and those at the terminal stage of disease. The gap in infectivity levels between these two groups was around 10-fold; 10-fold dilution of the samples from the cpd-B-treated terminal mice similarly produced no signals on the immunoblot, as observed in the samples from the cpd-B-treated mice at day 63 postinfection (data not shown).

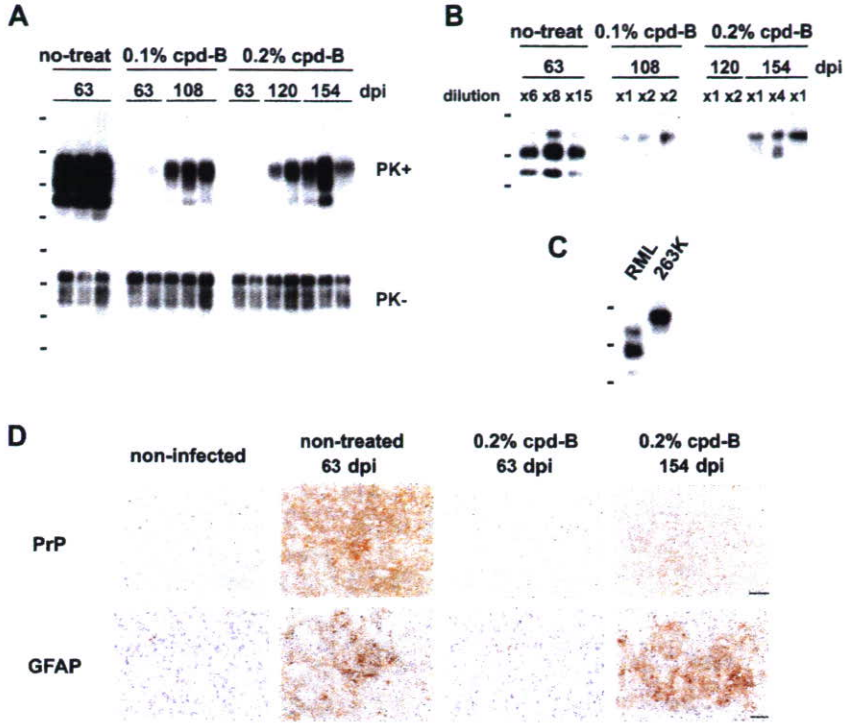

FIG. 4. Immunoblot and immunohistochemical analyses of cpd-B-treated animal brains. (A) Immunoblot analysis of PrP in the brains of nontreated mice (no-treat) or mice treated with 0.1% cpd-B feed or 0.2% cpd-B feed. Each lane represents an aliquot corresponding to 0.13 mg for PrPres (PK+) or 0.83 μg for total PrP (PK−) of brain tissue from each mouse sacrificed at a designated day after cerebral infection (dpi). Molecular size markers on the left show 47, 32, 25, and 16 kDa. (B) Immunoblot analysis of PrPres of some of the samples in panel A, which were diluted and reassayed to equalize signal intensities of the diglycosylated PrPres bands as much as possible for comparison of the signal intensity and the glycoform pattern of PrPres. Molecular size markers on the left show 32, 25, and 16 kDa. (C) Immunoblot analysis of PrPres to compare the glycoform patterns of the RML prion and the 263K prion. Analyzed samples were from an RML prion-infected mouse brain and a 263K prion-infected hamster brain. Molecular size markers on the left are the same as those in panel B. (D) Immunohistochemical analysis of abnormal PrP deposition (PrP) and neurodegenerative changes by means of astrocytic glial reaction (glial fibrillary acidic protein [GFAP]) in the brains of noninfected mice, infected but nontreated mice, and infected mice treated with 0.2% cpd-B feed. Data from each representative mouse sacrificed at a designated day after cerebral infection (dpi) are shown; every picture was taken from an almost identical area of the thalamus. The samples of 0.2% cpd-B at 63 dpi and 0.2% cpd-B at 154 dpi are from the same individual mouse as the samples in the right lane of 0.2% cpd-B 63 dpi and the rightmost lane of 0.2% cpd-B 154 dpi in panel A, respectively. Bar, 50 μm.

DISCUSSION

In this study, the newly synthesized chemical cpd-B was discovered as an orally available antiprion compound that is effective for prolonging the incubation periods of animals cerebrally infected with prion diseases. This compound has no similarity in chemical structure to previously reported antiprion compounds, although the compound shares the following properties with antiprion amyloidophilic chemicals we previously reported, such as (*trans*, *trans*)-1-bromo-2,5-bis-(3-hydroxycarbonyl-4-hydroxy)styrylbenzene and styrylbenzoazole chemicals: binding to PrP amyloid plaques in the brain tissue, inhibiting abnormal PrP formation in prion-infected cells without any effect on either normal PrP expression level or protease sensitivity of abnormal PrPres, preferential antiprion effects in RML prion-infected cells rather than 22L prion-infected or Fukuoka-1 prion-infected cells, and prolonging the incubation period in the RML prion-infected Tga20 mouse model but never or only marginally in the 263K prion-infected Tg7 mouse model. The discovery of orally available cpd-B effectiveness reinforces the idea that amyloidophilic chemicals can serve as one class of antiprion drug candidates.

This study has shown that prion strains are definitely influential in the outcome of the treatment with antiprion compounds. Treatment with cpd-B was effective against all tested prion strains, but both its antiprion effectiveness in vitro and its therapeutic efficacy in vivo were consistently dependent on the prion strain. In fact, cpd-B was most effective against RML prion but less effective against 22L prion and Fukuoka-1 prion either in vitro or in vivo. In addition, its lowest effectiveness in therapeutic efficacy was demonstrated identically in either the 263K prion-infected Tg7 mouse model or the 263K prion-infected hamster model, although its effectiveness against 263K prion could not be evaluated on the same host background as that used for the other prion strains. It is unlikely that differences in the hosts used in this study are influential in the therapeutic efficacy of cpd-B treatment, because the brain chemical levels in all types of mice fed with 0.2% cpd-B for 1 week were not significantly different.

Amyloidophilic chemicals are not the only class of antiprion compound that exhibits the therapeutic efficacy in a prion strain-dependent manner. The polyene antibiotic amphotericin B is another example, but it is opposite to amyloidophilic chemicals and is specifically effective against 263K prion (1).

TABLE 2. Infectivity assays of the brains of nontreated mice or cpd-B-treated mice

Dilution	Nontreated mice (63 dpi[a])			cpd-B treated mice (63 dpi)			cpd-B treated mice (154 dpi)		
	Mouse no.	No. of diseased mice/total	Mean incubation time (days) ± SD	Mouse no.	No. of diseased mice/total	Mean incubation time (days) ± SD	Mouse no.	No. of diseased mice/total	Mean incubation time (days) ± SD
10^2	cnt-1	8/8	77.4 ± 4.5	bc-1[d]	7/7	284.1 ± 54.6	bl-1	7/7	122.0 ± 14.0
				bc-2[e]	8/8	136.8 ± 19.2	bl-2[f]	7/7	92.6 ± 8.9
							bl-3	7/7	89.1 ± 4.0
10^3	cnt-1	8/8	84.4 ± 6.9	bc-1[d]	0/7	>140[c]	bl-1	5/9	>140[c]
	cnt-2	6/6	75.3 ± 2.4	bc-2[e]	1/8	>140[c]	bl-2[f]	7/7	97.4 ± 9.6
	cnt-3	7/7	75.7 ± 7.4				bl-3	9/9	101.6 ± 7.4
10^4	cnt-1	7/7	88.4 ± 7.3	bc-1[d]	1/8	>140[c]	bl-1	1/9	>140[c]
				bc-2[e]	1/9	>140[c]	bl-2[f]	3/7	>140[c]
							bl-3	3/7	>140[c]
10^5	cnt-1	6/6	155.7 ± 55.3						
	cnt-2	7/7	105.4 ± 16.5						
	cnt-3	7/7	95.9 ± 7.1						
10^6	cnt-1	1/7	>420[b]						
10^7	cnt-1	3/7	>420[b]						
10^8	cnt-1	1/7	>420[b]						
10^9	cnt-1	2/7	>420[b]						

[a] Days after cerebral inoculation.
[b] Observed up to 420 days postinoculation.
[c] Observed up to 140 days postinoculation.
[d] Mouse for the sample in the left lane of 0.2% cpd-B at 63 dpi in Fig. 4A.
[e] Mouse for the sample in the right lane of 0.2% cpd-B at 63 dpi in Fig. 4A.
[f] Mouse for the sample of the rightmost lane of 0.2% cpd-B at 154 dpi in Fig. 4A.

Either variation in strain-specific PrP conformational structures or variation in microenvironments facilitating PrP conformational changes might be involved in the mechanism of prion strain-dependent efficacy. The results of this study showed that prions producing predominantly diglycosylated PrPres molecules were least sensitive or resistant to cpd-B treatment, which suggests that either the conformational structure responsible for PrPres or the diglycosylation moieties might affect the interaction of the compound with abnormal PrP molecules, although this inference must be examined further. The findings indicate that each class of antiprion compounds must be examined using various prion strains to learn more about prion strain dependency.

Even in the terminal stage of disease, both abnormal PrP deposition levels in the brain and infectivity levels in the brain were reduced in the mice treated with cpd-B compared to the nontreated control mice. It remains unclear why this gap occurs. One possibility is that the treated mice prematurely fell into the terminal stage because of accumulated cpd-B toxicity. This inference, however, does not seem to be correct, because the noninfected mice treated with 0.2% cpd-B feed for more than 1 year showed no clinical signs and appeared healthy. Another possibility is that neuronal cells in the brain might be more vulnerable to lower levels of abnormal PrP in the presence of cpd-B or that abnormal PrP bound with cpd-B might be more toxic to the neuronal cells in the brain. However, these inferences also seem to be unlikely, because the toxicity of PrP106-126 peptide amyloid, which is reminiscent of abnormal PrP, in primary neuronal cell cultures is attenuated by the presence of cpd-B (unpublished data). Another possibility is that prion strains modified or selected from the original by the compound might multiply in the animals and cause the disease; this inference is supported by data showing that PrPres molecules with different glycoform patterns were detected in the treated mice. Further study, however, must provide evidence to support this inference. The findings indicate that life-threatening levels of either infectivity or abnormal PrP in the brain are not necessarily the same between treated animals and nontreated animals.

A large quantity of cpd-B was needed for efficacy in vivo; disease progression was not halted even though the treatment commenced immediately after the infection and continued to the terminal stage of disease. This limited effectiveness of cpd-B might be partly attributable to the pharmacological properties of its rapid washout from either the brain or the blood, because it is assumed that the compounds with better brain permeativity and longer retention in the brain might produce more beneficial results in prion-infected animals. In addition, some metabolic instability of the compound might be responsible for its limited effectiveness, especially the loss of efficacy during long-term administration. In fact, cpd-B is easily metabolized in the presence of mouse liver microsome extracts (unpublished data). Therefore, the pharmacokinetic parameters of this compound must be improved for better efficacy.

The effectiveness of cpd-B is dependent upon the timing and duration of administration; an earlier start of administration is

necessary to maximize beneficial results. Therefore, diagnostic measures in much earlier disease stages, especially presymptomatic stages, are vital to produce more beneficial outcomes. In addition, multidrug combination chemotherapy using several antiprion compounds with different actions might produce more beneficial results. This study suggests that cpd-B inhibits new formation of abnormal PrP but does not facilitate the degradation of already formed abnormal PrP, because a mixture of cpd-B with abnormal PrP did not modify the protease-resistant property of abnormal PrP. In addition, cpd-B itself has no activity to protect neuronal cells from neurotoxic insults aside from PrP amyloid (unpublished data), suggesting that cpd-B does not protect neuronal cells from neurodegenerative insults that are induced secondarily by abnormal PrP. Combinations of cpd-B with other compounds such as doxycycline, flupirtine, and simvastatin might be examples, but their efficacy must be evaluated. Doxycycline is a tetracycline antibiotic known to destabilize abnormal PrP (12). Flupirtine is a centrally acting nonopioid analgesic and protects neuronal cells from apoptotic cell death induced by toxic PrP106-126 peptide amyloid (29). It was used in clinical trials, where beneficial effects on cognitive functions in patients with CJD were proved (21). Simvastatin is a cholesterol-lowering drug known to prevent abnormal PrP formation in prion-infected cells, presumably by redistribution of normal PrP away from cholesterol-rich lipid rafts (13, 31). It prolongs survival times in prion-infected animals (16, 17).

Recently, long-term cerebroventricular administration of pentosan polysulfate (PPS), a clinical approach based on our preclinical study in rodent models of prion diseases (9), has been carried out in 26 patients with various types of diseases (27). Although its therapeutic efficacy remains to be confirmed, preliminary clinical experience indicates prolonged survival in some patients receiving long-term PPS (22, 27). Further prospective investigation of PPS administration is necessary to obtain high-quality evidence for its clinical benefits. However, this treatment has some weaknesses. One is the requirement for surgical implantation of a continuous infusion pump and an intraventricular catheter, which could become an obstacle to extension of clinical trials because of the potential risks of prion contamination in operating rooms and of operation instruments, although most developed countries now possess clearly defined and well established guidelines for safe surgical and anesthetic management of patients with prion diseases. Compared to such treatments, the treatments using orally available antiprion compounds are absolutely preferable and practical.

The compounds tested in the study were originally designed as therapeutic lead chemicals for the treatment of Alzheimer's disease. In fact, cpd-B and related chemicals are very effective in vitro in either inhibiting beta-amyloid formation or protecting neuronal cells from beta-amyloid toxicity; in addition, cpd-B has therapeutic efficacy in an Alzheimer's disease mouse model (unpublished data). Therefore, cpd-B is a therapeutic candidate not only for prion diseases but also for Alzheimer's disease. The search for and development of drugs for prion diseases reportedly do not interest pharmaceutical companies because of the limited number of patients, but the possible use of amyloidophilic chemicals as drug candidates for both prion diseases and Alzheimer's disease might attract and accelerate the development of therapeutic drugs for prion diseases.

In conclusion, our findings related to the newly synthesized amyloidophilic chemical cpd-B are encouraging, but further improvement of its safety profiles and pharmacokinetic properties is necessary before clinical application can be considered. Moreover, additional problems exist with its prion strain-dependent effectiveness and with its reduced effectiveness if administered at later disease stages.

ACKNOWLEDGMENTS

This work was supported by grants from the Japanese Ministry of Health, Labor and Welfare (H16-kokoro-024 and H19-nanji-006); the Japanese Ministry of Agriculture, Forestry and Fisheries; and the Japan Society for the Promotion of Science (A2-14207030 and B-19390234).

We thank Kayoko Motoki, Takashi Odagiri, and Tetsuya Mimura from Daiichi Pharmaceutical Co., Ltd., for synthesis of the amyloidophilic compounds tested in the study; Yuki Yamada and Hiroto Akama from Tohoku University for technical assistance; and Tetsuyuki Kitamoto and Yukitsuka Kudo from Tohoku University for helpful suggestions.

REFERENCES

1. **Adjou, K. T., J. P. Deslys, R. Demaimay, and D. Dormont.** 1997. Probing the dynamics of prion diseases with amphotericin B. Trends Microbiol. **5**:27–31.
2. **Bresjanac, M., L. M. Smid, T. D. Vovko, A. Petric, J. R. Barrio, and M. Popovic.** 2003. Molecular-imaging probe 2-(1-[6-[(2-fluoroethyl)(methyl)-amino]-2-naphthyl]ethylidene)malononitrile labels prion plaques in vitro. J. Neurosci. **23**:8029–8033.
3. **Cai, L., R. B. Innis, and V. W. Pike.** 2007. Radioligand development for PET imaging of beta-amyloid (Abeta)—current status. Curr. Med. Chem. **14**: 19–52.
4. **Cashman, N. R., and B. Caughey.** 2004. Prion diseases—close to effective therapy? Nat. Rev. Drug Discov. **3**:874–884.
5. **Caughey, B., and R. E. Race.** 1992. Potent inhibition of scrapie-associated PrP accumulation by Congo red. J. Neurochem. **59**:768–771.
6. **Caughey, B., and G. J. Raymond.** 1993. Sulfated polyanion inhibition of scrapie-associated PrP accumulation in cultured cells. J. Virol. **67**:643–650.
7. **Doh-ura, K., E. Mekada, K. Ogomori, and T. Iwaki.** 2000. Enhanced CD9 expression in the mouse and human brains infected with transmissible spongiform encephalopathies. J. Neuropathol. Exp. Neurol. **59**:774–785.
8. **Doh-Ura, K., T. Iwaki, and B. Caughey.** 2000. Lysosomotropic agents and cysteine protease inhibitors inhibit scrapie-associated prion protein accumulation. J. Virol. **74**:4894–4897.
9. **Doh-ura, K., K. Ishikawa, I. Murakami-Kubo, K. Sasaki, S. Mohri, R. Race, and T. Iwaki.** 2004. Treatment of transmissible spongiform encephalopathy by intraventricular drug infusion in animal models. J. Virol. **78**:4999–5006.
10. **Doh-Ura, K., T. Kuge, M. Uomoto, K. Nishizawa, Y. Kawasaki, and M. Iha.** 2007. Prophylactic effect of dietary seaweed fucoidan against enteral prion infection. Antimicrob. Agents Chemother. **51**:2274–2277.
11. **Fischer, M., T. Rulicke, A. Raeber, A. Sailer, M. Moser, B. Oesch, S. Brandner, A. Aguzzi, and C. Weissmann.** 1996. Prion protein (PrP) with amino-proximal deletions restoring susceptibility of PrP knockout mice to scrapie. EMBO J. **15**:1255–1264.
12. **Forloni, G., S. Iussich, T. Awan, L. Colombo, N. Angeretti, L. Girola, I. Bertani, G. Poli, M. Caramelli, M. Grazia Bruzzone, L. Farina, L. Limido, G. Rossi, G. Giaccone, J. W. Ironside, O. Bugiani, M. Salmona, and F. Tagliavini.** 2002. Tetracyclines affect prion infectivity. Proc. Natl. Acad. Sci. USA **99**:10849–10854.
13. **Gilch, S., C. Kehler, and H. M. Schatzl.** 2006. The prion protein requires cholesterol for cell surface localization. Mol. Cell Neurosci. **31**:346–353.
14. **Ishikawa, K., K. Doh-ura, Y. Kudo, N. Nishida, I. Murakami-Kubo, Y. Ando, T. Sawada, and T. Iwaki.** 2004. Amyloid imaging probes are useful for detection of prion plaques and treatment of transmissible spongiform encephalopathies. J. Gen. Virol. **85**:1785–1790.
15. **Ishikawa, K., Y. Kudo, N. Nishida, T. Suemoto, T. Sawada, T. Iwaki, and K. Doh-ura.** 2006. Styrylbenzoazole derivatives for imaging of prion plaques and treatment of transmissible spongiform encephalopathies. J. Neurochem. **99**:198–205.
16. **Kempster, S., C. Bate, and A. Williams.** 2007. Simvastatin treatment prolongs the survival of scrapie-infected mice. Neuroreport **18**:479–482.
17. **Mok, S. W., K. M. Thelen, C. Riemer, T. Bamme, S. Gultner, D. Lutjohann, and M. Baier.** 2006. Simvastatin prolongs survival times in prion infections of the central nervous system. Biochem. Biophys. Res. Commun. **348**:697–702.
18. **Murakami-Kubo, I., K. Doh-Ura, K. Ishikawa, S. Kawatake, K. Sasaki, J.**

Kira, S. Ohta, and T. Iwaki. 2004. Quinoline derivatives are therapeutic candidates for transmissible spongiform encephalopathies. J. Virol. **78**:1281–1288.

19. **Okamura, N., T. Suemoto, H. Shimadzu, M. Suzuki, T. Shiomitsu, H. Akatsu, T. Yamamoto, M. Staufenbiel, K. Yanai, H. Arai, H. Sasaki, Y. Kudo, and T. Sawada.** 2004. Styrylbenzoxazole derivatives for in vivo imaging of amyloid plaques in the brain. J. Neurosci. **24**:2535–2541.
20. **Okamura, N., T. Suemoto, S. Furumoto, M. Suzuki, H. Shimadzu, H. Akatsu, T. Yamamoto, H. Fujiwara, M. Nemoto, M. Maruyama, H. Arai, K. Yanai, T. Sawada, and Y. Kudo.** 2005. Quinoline and benzimidazole derivatives: candidate probes for in vivo imaging of tau pathology in Alzheimer's disease. J. Neurosci. **25**:10857–10862.
21. **Otto, M., L. Cepek, P. Ratzka, S. Doehlinger, I. Boekhoff, J. Wiltfang, E. Irle, G. Pergande, B. Ellers-Lenz, O. Windl, H. A. Kretzschmar, S. Poser, and H. Prange.** 2004. Efficacy of flupirtine on cognitive function in patients with CJD: a double-blind study. Neurology **62**:714–718.
22. **Parry, A., I. Baker, R. Stacey, and S. Wimalaratna.** 2007. Long term survival in a patient with variant Creutzfeldt-Jakob disease treated with intraventricular pentosan polysulphate. J. Neurol. Neurosurg. Psychiatry **78**:733–734.
23. **Prusiner, S. B., M. P. McKinley, K. A. Bowman, D. C. Bolton, P. E. Bendheim, D. F. Groth, and G. G. Glenner.** 1983. Scrapie prions aggregate to form amyloid-like birefringent rods. Cell **35**:349–358.
24. **Prusiner, S. B.** 1991. Molecular biology of prion diseases. Science **252**:1515–1522.
25. **Race, R. E., B. Caughey, K. Graham, D. Ernst, and B. Chesebro.** 1988. Analyses of frequency of infection, specific infectivity, and prion protein biosynthesis in scrapie-infected neuroblastoma cell clones. J. Virol. **62**:2845–2849.
26. **Race, R. E., S. A. Priola, R. A. Bessen, D. Ernst, J. Dockter, G. F. Rall, L. Mucke, B. Chesebro, and M. B. Oldstone.** 1995. Neuron-specific expression of a hamster prion protein minigene in transgenic mice induces susceptibility to hamster scrapie agent. Neuron **15**:1183–1191.
27. **Rainov, N. G., Y. Tsuboi, P. Krolak-Salmon, A. Vighetto, and K. Doh-Ura.** 2007. Experimental treatments for human transmissible spongiform encephalopathies: is there a role for pentosan polysulfate? Expert Opin. Biol. Ther. **7**:713–726.
28. **Sadowski, M., J. Pankiewicz, H. Scholtzova, J. Tsai, Y. Li, R. I. Carp, H. C. Meeker, P. Gambetti, M. Debnath, C. A. Mathis, L. Shao, W. B. Gan, W. E. Klunk, and T. Wisniewski.** 2004. Targeting prion amyloid deposits in vivo. J. Neuropathol. Exp. Neurol. **63**:775–784.
29. **Schroder, H. C., and W. E. Muller.** 2002. Neuroprotective effect of flupirtine in prion disease. Drugs Today **38**:49–58.
30. **Smid, L. M., T. D. Vovko, M. Popovic, A. Petric, V. Kepe, J. R. Barrio, G. Vidmar, and M. Bresjanac.** 2006. The 2,6-disubstituted naphthalene derivative FDDNP labeling reliably predicts Congo red birefringence of protein deposits in brain sections of selected human neurodegenerative diseases. Brain Pathol. **16**:124–130.
31. **Taraboulos, A., M. Scott, A. Semenov, D. Avrahami, L. Laszlo, and S. B. Prusiner.** 1995. Cholesterol depletion and modification of COOH-terminal targeting sequence of the prion protein inhibit formation of the scrapie isoform. J. Cell Biol. **129**:121–132.
32. **Trevitt, C. R., and J. Collinge.** 2006. A systematic review of prion therapeutics in experimental models. Brain **129**:2241–2265.

J Neurol (2007) 254:1509–1517
DOI 10.1007/s00415-007-0540-9

ORIGINAL COMMUNICATION

Two different clinical phenotypes of Creutzfeldt-Jakob disease with a M232R substitution

Yusei Shiga · Akira Satoh · Katsuya Satoh · Yoshito Matsuda · Tetsuyuki Kitamoto · Mitsuru Hidaka · Sigenori Kanno · Hirokatsu Takahashi · Ichiro Nakashima · Yasuteru Sano · Shigeru Sato · Kang Kim · Kazuo Fujihara · Takashi Konishi · Hiroshi Takata · Katsumi Doh-ura · Keigo Nobukuni · Takeshi Sato · Shigetoshi Kuroda · Kensuke Sasaki · Hiroki Takano · Yoshikazu Nakamura · Yoshitaka Umeda · Masahito Yamada · Hidehiko Konno · Hidehiro Mizusawa · Kunihiko Nagasato · Yasuto Itoyama

Received: 28 June 2006
Received in revised form: 8 January 2007
Accepted: 6 February 2007
Published online: 2 November 2007

Y. Shiga, MD, PhD* (✉) · S. Kanno, MD · I. Nakashima, MD, PhD · K. Fujihara, MD, PhD · Y. Itoyama, MD, PhD
Dept. of Neurology
Tohoku University Graduate School of Medicine
1-1 Seiryo-machi, Aoba-ku
Sendai 980-8574, Japan
Tel.: +81-22/717-7189
Fax: +81-22/717-7192
E-Mail:
yshiga@em.neurol.med.tohoku.ac.jp

K. Satoh, MD, PhD
The First Department of Internal Medicine
Graduate School of Medicine
Nagasaki University, Japan

T. Kitamoto, MD, PhD*
Division of CJD Science and Technology
Graduate School of Medicine
Tohoku University, Japan

S. Sato, MD, PhD
Dept. of Neurology
Kohnan Hospital, Japan

H. Takata, MD, PhD · K. Nobukuni, MD, PhD
Dept. of Neurology
Minami Okayama National Hospital, Japan

S. Kuroda, MD, PhD*
Dept. of Neuropsychiatry
Graduate School of Medicine, Dentistry and Pharmaceutical Sciences
Okayama University, Japan

H. Takano, MD, PhD · Y. Umeda, MD, PhD
Dept. of Neurology
Brain Research Institute
Niigata University, Japan

H. Konno, MD, PhD
Dept. of Neurology
Nishitaga National Hospital, Japan

K. Nagasato, MD, PhD
Dept. of Neurology
Isahaya General Hospital, Japan

A. Satoh, MD, PhD
Dept. of Neurology
Nagasaki Kita Hospital, Japan

Y. Matsuda, MD, PhD
Dept. of Neuropsychiatry
Graduate School of Medicine
Yamaguchi University, Japan

M. Hidaka, MD, PhD
Yokohama Miyazaki Hospital of Neurosurgery, Japan

H. Takahashi, MD, PhD
Dept. of Neurology
Matsudo Municipal Hospital, Japan

Y. Sano, MD, PhD
Dept. of Neurology
Graduate School of Medicine
Yamaguchi University, Japan

K. Kim, MD, PhD
Dept. of Neurology
Shizuoka General Hospital, Japan

T. Konishi, MD, PhD
Dept. of Neurology
Shizuoka National Medical Center, Japan

K. Doh-ura, MD, PhD
Division of Prion Protein Biology
Graduate School of Medicine
Tohoku University, Japan

T. Sato, MD, PhD*
National Center for Neurology and Psychiatry
Kohnodai Hospital, Japan

K. Sasaki, MD, PhD
Dept. of Neuropathology
Neurological Institute
Graduate School of Medical Sciences
Kyushu University, Japan

Y. Nakamura, MD, PhD*
Dept. of Public Health
Jichi Medical School, Japan

M. Yamada, MD, PhD*
Depts. of Neurology and Neurobiology of Aging
Graduate School of Medical Science
Kanazawa University, Japan

H. Mizusawa, MD, PhD*
Dept. of Neurology and Neurological Science
Graduate School
Tokyo Medical and Dental University, Japan

* The Creutzfeldt-Jakob Disease Surveillance Committee, Japan.

JON 2540

☐ **Abstract** *Objective* To describe the clinical features of Creutzfeldt-Jakob disease with a substitution of arginine for methionine (M232R substitution) at codon 232 (CJD232) of the prion protein gene (PRNP). *Patients and methods* We evaluated the clinical and laboratory features of 20 CJD232 patients: age of onset, initial symptoms, duration until becoming akinetic and mute, duration until occurrence of periodic sharp and wave complexes on EEG (PSWC), MRI findings, and the presence of CSF 14-3-3 protein. Immunohistochemically, prion protein (PrP) deposition was studied. *Results* None of the patients had a family history of CJD. We recognized two clinical phenotypes: a rapidly progressive type (rapid-type) and a slowly progressive type (slow-type). Out of 20 patients, 15 became akinetic and mute, demonstrated myoclonus, and showed PSWC within a mean duration of 3.1, 2.4, and 2.8 months, respectively (rapid-type). Five showed slowly progressive clinical courses (slow-type). Five became akinetic and mute and four demonstrated myoclonus within a mean duration of 20.6 and 15.3 months, respectively, which were significantly longer than those in the rapid-type. Only one demonstrated PSWC 13 months after the onset. Diffuse synaptic-type deposition was demonstrated in four rapid-type patients, and perivacuolar and diffuse synaptic-type deposition in two, and diffuse synaptic-type deposition in one slow-type patient. Three of 50 suspected but non-CJD patients had the M232R substitution. *Conclusions* Patients with CJD232 had no family history like patients with sCJD, and showed two different clinical phenotypes in spite of having the same PRNP genotype. More studies are needed to determine whether M232R substitution causes the disease and influences the disease progression.

☐ **Key words** Creutzfeldt-Jakob disease · M232R · clinical phenotype · uncommon variant · diffusion-weighted MRI

Introduction

Human prion diseases are divided into three types: sporadic, genetic, and infectious prion disease. Genetic prion disease, which is defined as prion disease with causative abnormalities of the prion protein gene (PRNP), accounts for approximately 10 to 15% of all prion disease cases, and includes genetic Creutzfeldt-Jakob disease (gCJD), Gerstmann-Sträussler-Scheinker disease (GSS), and fatal familial insomnia (FFI) [1]. In general, the clinical features of gCJD are more various compared with those of sporadic CJD (sCJD) and are regulated by the genotype [2]. Therefore, gCJD, even if its clinical features are quite different from those of sCJD, especially those of the most often encountered type of sCJD with methionine homozygosity at codon 129 of PRNP and type 1 protease-resistant prion protein (MM1) [3], can be diagnosed by examining the genotype. To clarify the clinical features of CJD, which associates with a substitution in PRNP, will provide an important clue that can lead to genetic examination.

To date, more than 30 causative mutations have been recognized and individual PRNP mutations show variable geographical distribution and frequency. The cardinal characteristic of gCJD is that more than half of the patients lack family history.

CJD patients associated with a substitution of arginine for methionine at codon 232 (M232R substitution) in PRNP with no relevant family history have been reported in Japan [4–10]. Previously, the clinical features of CJD with the M232R substitution (CJD232) were thought to be similar to those of typical sCJD with MM1 [3], which accounts for the vast majority of sCJD in terms of clinical features, including EEG findings [5, 6, 9]. However, cases of CJD232 that showed a longer clinical course and lacked the characteristic periodic sharp and wave complexes (PSWC) have been reported [7, 8]. We have experienced eight cases of CJD232. Five of them showed a rapid clinical course and typical CJD features, while the others showed very slow progression and atypical features. We studied the clinical features of 20 CJD232 patients, including our original patients, and found that there were two different major clinical phenotypes with the same genotype, including polymorphisms at codons 129 and 219 of PRNP; one progressed rapidly, and the other progressed slowly. Better understanding of the clinical features of CJD232 would contribute to the diagnosis of CJD232, especially in patients with atypical clinical features.

Patients and methods

Twenty-four patients with CJD232 were included in this study: eight were our original cases, seven were obtained by reviewing the literature [5–10] and nine were found by reviewing the clinical records of CJD patients reported to the Creutzfeldt-Jakob disease Surveillance Committee, Japan. We excluded two patients because they had double point mutations at codon 180 and at codon 232 [10] and one patient because her polymorphism at codons 129 and 219 of PRNP was uncertain [5]. Therefore, 21 patients were enrolled in this study. The nine who were proven at autopsy are indicated by asterisks in Fig. 1.

We first evaluated the duration from onset until the patients manifested akinetic mutism. As shown in Fig. 1, 15 became akinetic and mute within six months, while five did not become so until 15 months after the onset. These CJD232 patients appeared to be comprised of two different groups: one was a rapidly progressive type (rapid-type) and the other was a slowly progressive type (slow-type). We evaluated the age of onset, initial symptoms, duration from onset to the appearance of myoclonus, duration from onset to akinetic mutism, du-

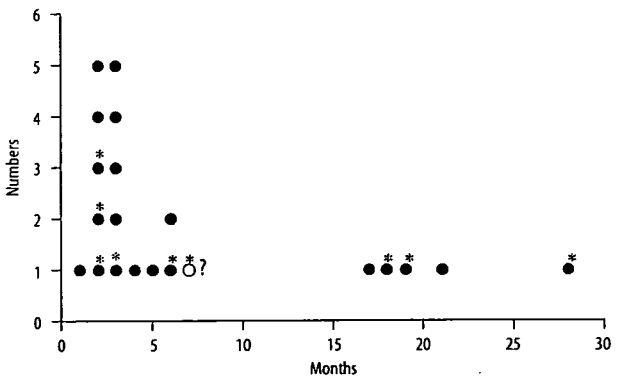

Fig. 1 The duration from the onset to akinetic mutism. The X-axis shows the duration (months) and the Y-axis shows the accumulative number of patients. Black circles indicate patients who became akinetic and mute; the white circle indicates a patient who had not become akinetic and mute. The white circle with a question mark indicates a 50-year-old-male patient who suddenly died seven months after the onset because of a myocardial incident. Since he had not become akinetic and mute, and was able to converse with simple words, we excluded him from further analyses. Asterisks indicate autopsy proven patients. We recognize two different groups concerning the duration from the onset to akinetic mutism: a rapidly progressive type and a slowly progressive type

ration from onset to occurrence of PSWC, results of MRI, and the presence of 14-3-3 protein in the CSF of the two types. The patient marked by a question mark in Fig. 1 was excluded from the evaluation. We were unable to determine which group this 50-year-old man belonged to because he had not become akinetic and mute and was still able to converse with simple words seven months after the onset when he suddenly died due to a myocardial incident [8]. Thus, the clinical data of 20 patients were finally used for this study.

In one of the rapid-type patients and in three of the slow-type patients including a previously reported 64-year-old woman [7], immunohistochemical staining of PrP using monoclonal antibody 3F4 (Prionics, Schlieren, Switzerland) was performed. Including the previously reported pathological findings of three patients belonging to the rapid-type [6], immunohistochemical staining of PrP in both groups were studied. In each group, the molecular type of the abnormal isoform of prion protein (PrP^{Sc}) was studied.

The Mann-Whitney U test was used for statistical comparison of the age of onset and the duration until the appearance of myoclonus and akinetic mutism from the onset between the rapid-type and the slow-type. The Grubbs-Smirnov critical test was used for statistical analysis of the duration until the appearance of PSWC from the onset between the rapid-type and the slow-type. Fisher's exact probability test was used for comparison of the male to female ratio, and the rates of myoclonus, akinetic mutism, and PSWC between the two types. It was also used for comparison of the positive rate of 14-3-3 immunoassay and MRI between the two types.

Results

Reviewing the clinical records of the enrolled patients, we found that no patients of either group had a family history of prion disease or dementia.

Fifteen patients, eight men and seven women, with a mean onset age of 65.4 ± 5.2 (Mean ± SD) years could be categorized as the rapid-type. Of those, seven with an initial symptom of progressive dementia or memory disturbance, two with visual symptoms, two with cerebellar ataxia, two with involuntary movement, and two with other symptoms. All except for one uncertain patient demonstrated myoclonus 2.4 ± 1.8 months after the onset. All became akinetic and mute within a mean duration of 3.1 ± 1.5 months, and demonstrated PSWC (Fig. 2A and B) within a mean duration of 2.8 ± 1.8 months. CJD-related high intensity lesions [11] were detected in eight of the nine patients examined by MRI. Similar to sCJD, three patterns existed: in one, high intensity lesions appeared mainly in the striatum (Fig. 3A); in another, they appeared in the striatum and the cortical ribbon equally (Fig. 3B); and in yet another, they appeared mainly in the cortical ribbon (Fig. 3C). The 14-3-3 protein assay was positive in all eight patients examined. All 15 patients showed MM129, 14 showed glutamic acid homozygosity at codon 219 (GG219) and one showed glutaminic acid/lysine heterozygosity at codon 219 in the PRNP analysis. These clinical features closely resembled typical sCJD with MM1 [3]. Immunohistochemical staining of PrP in four patients (one original patient and three previously reported patients [6]) revealed a diffuse synaptic-type deposit (Fig. 4A). The molecular type of PrP^{Sc} in one patient was type 1.

Five patients, two men and three women, with a mean onset age of 59.0 ± 12.8 years could be categorized as the slow-type. Three had an initial symptom of progressive dementia or memory disturbance, one showed psychiatric symptoms, and one had dressing apraxia. Four of five patients demonstrated myoclonus 15.3 ± 12.3 months after the onset, and the remaining one did not demonstrate myoclonus during the 13-month observation period. All became akinetic and mute within a mean duration of 20.6 ± 4.4 months. Only one demonstrated PSWC within the observation period of 23.8 ± 13.7 months (Fig. 2C and 2D). CJD-related high-intensity lesions were detected in four of the five patients examined by MRI [11]. One showed high-intensity lesions in the cortical ribbon (Fig. 3D and 3E), while in the others such lesions appeared in both the striatum and cortical ribbon (Fig. 3F). The medial thalami showed high-intensity lesions in all three patients examined by DWI (white arrows in Fig. 3D and E, and black arrows in Fig. 3F). The 14-3-3 protein assay was positive in all four patients examined. In the PRNP analysis, all five patients showed MM129 and GG219. Immunohistochemical staining in two patients revealed predominantly perivacuolar-type PrP deposits in the cerebral cortex (Fig. 4B), but also partly the diffuse synaptic-type deposits. In one patient, only the diffuse synaptic-type deposits were revealed. The molecular type of PrP^{Sc} in one patient who had predominantly perivacuolar-type PrP deposits was type 1 + 2.

Between the two groups, there were no differences in the age at onset, male to female ratio, or positive rate of

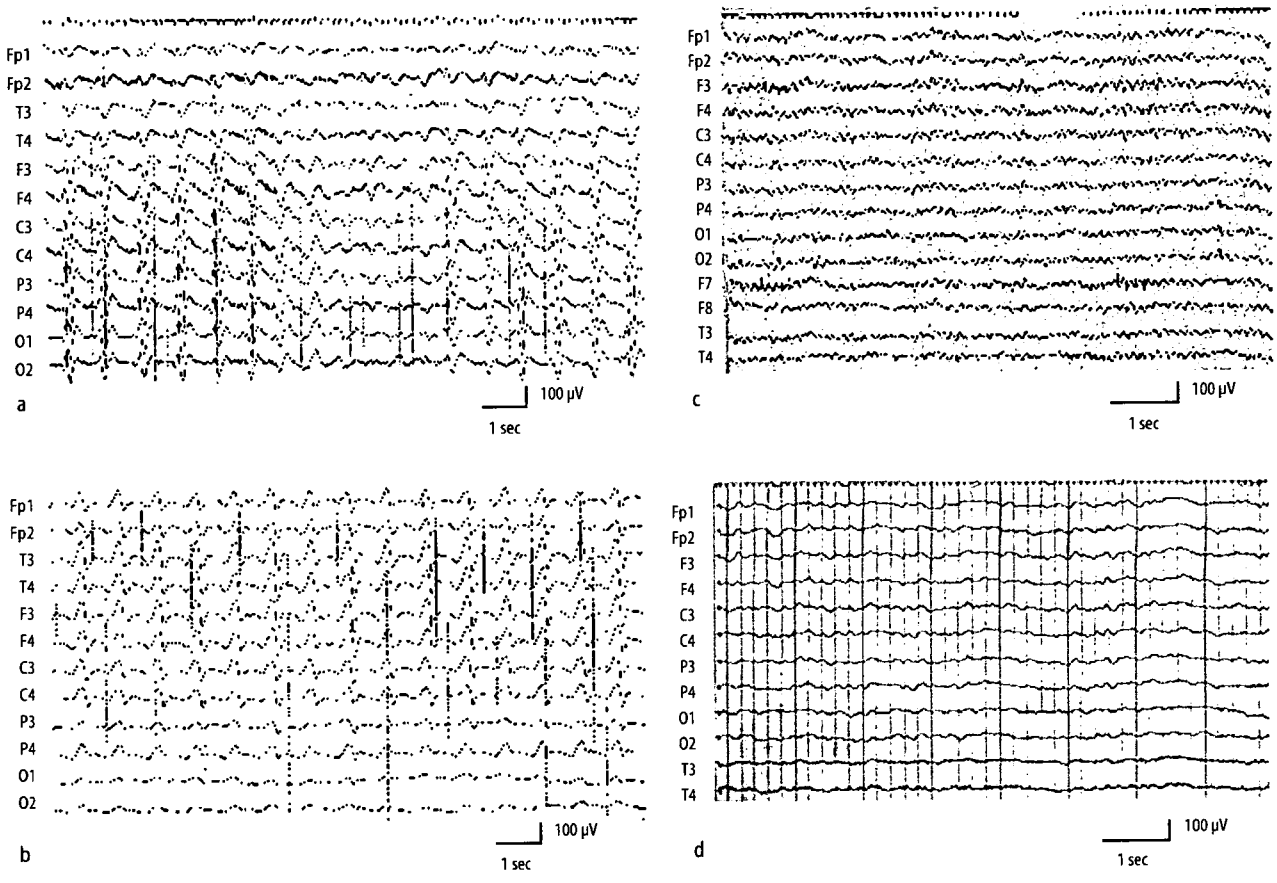

Fig. 2 EEG of representative patients of the rapid-type group and the slow-type group. **A** and **B** were recorded from the same 55-year-old woman in the rapid-type group. **C** and **D** were recorded from the same 69-year-old woman in the slow-type group. **A** EEG obtained two and half months after onset demonstrated high amplitude periodic sharp and wave complexes (PSWC) at a frequency of 1.5 Hz characteristic of CJD. **B** EEG obtained five months after the onset demonstrated PSWC at a frequency of 1 Hz. The amplitude was lower than that of Fig. 1A, and the background activities were flattened. EEG rapidly deteriorated. **C** EEG obtained four months after the onset. The background activities were 8 Hz mixed with no apparent slow activities. PSWC was not demonstrated. **D** EEG obtained twelve months after the onset. The background activities were 5 Hz mixed with δ activities. However, PSWC was not yet demonstrated

14-3-3 protein immunoassay. Similar to sCJD, there were three patterns of high-intensity lesions shown by MRI in the rapid-type. We were unable to distinguish the rapid-type of CJD232 from sCJD based on the clinical features including MRI findings. Patients with the slow-type did not have fewer lesions than patients with the rapid-type at diagnosis. High-intensity lesions in the medial thalamus depicted by DWI were a common finding of the slow-type (Fig. 3A–F). There was no difference in the rate of myoclonus between the two groups, but the duration until the appearance from the onset was longer in the slow-type compared with the rapid-type ($p < 0.005$). All patients became akinetic and mute in both types, but the duration until becoming akinetic and mute from the onset in the slow-type was longer than that in the rapid-type ($p < 0.001$). Concerning PSWC, all patients in the rapid-type demonstrated PSWC 2.8 ± 1.8 months after the onset. However, in the observation period of 21.6 ± 12.8 months, only one patient with the slow-type demonstrated PSWC 13 months after onset, which was later compared with that of the rapid-type ($p < 0.01$). The rate of PSWC in the slow-type was lower than that in the rapid-type ($p < 0.01$). Since there were no differences in the polymorphisms of codons 129 and 219 between the two groups, such polymorphisms would not be determinants of the disease subtype. Based on the differences in the clinical and laboratory findings (Table 1), we considered that these two types represented completely different phenotypes of exactly the same genotype.

By reviewing the investigative reports collected by the Creutzfeldt-Jakob Disease Surveillance Committee, Japan, as of February 2006, PRNP information was available from 511 patients: 317 were acknowledged as sporadic CJD, 41 as infectious CJD, 103 as genetic prion disease that included 28 CJD with V180I (CJD180), 27 GSS with P102L, 23 CJD with E200K, and 13 CJD232, and 50 as non-CJD. Three of the 50 non-CJD patients who had

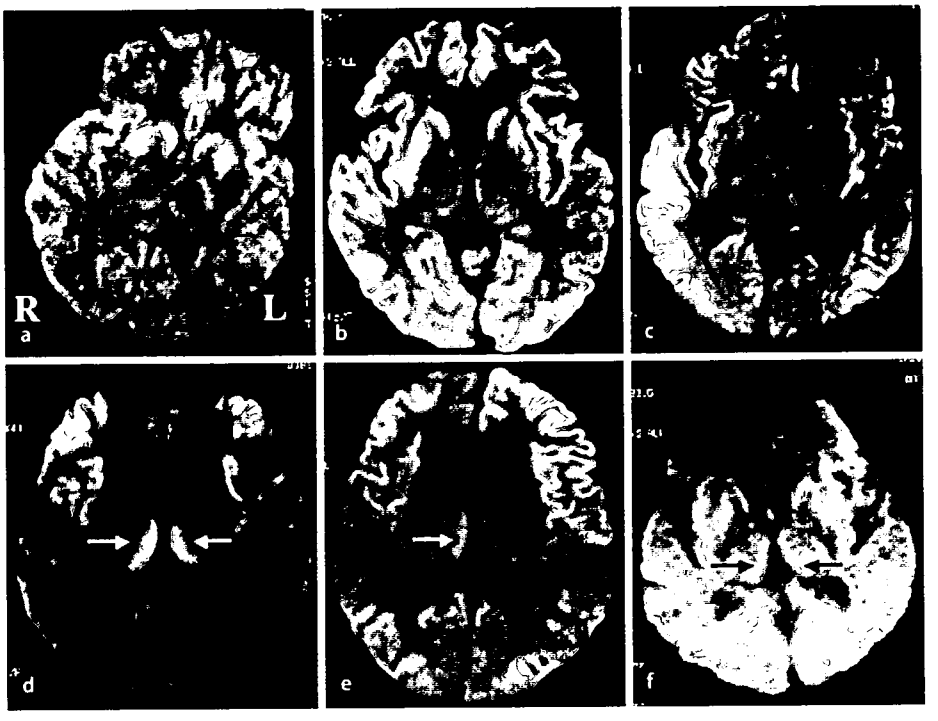

Fig. 3 DWI of the rapid-type group (**A–C**) and the slow-type group (**D–F**). **A** DWI obtained from a 55-year-old woman demonstrating high-intensity lesions mainly in the bilateral striatum. The right temporal cortex demonstrated slightly high-intensity lesions. **B** DWI obtained from a 60-year-old woman demonstrating high intensity lesions in the frontal, temporal, occipital and insular cortex, and the striatum. The right side predominated. **C** DWI obtained from a 62-year-old woman demonstrating high-intensity lesions in the bilateral occipital and insular cortex. The right temporal cortex was also depicted as an area of high intensity. We did not find high-intensity lesions in the striatum. **D** DWI obtained from a 69-year-old woman demonstrating high-intensity lesions in the bilateral frontal and insular cortex. The bilateral caudate head showed slightly high-intensity lesions. Interestingly, the bilateral medial thalami showed high-intensity lesions with the so-called hockey stick sign (white arrows). **E** DWI obtained from a 70-year-old man demonstrating high-intensity lesions in the bilateral frontal, occipital, and insular cortex. The right medial thalamus also showed high intensity (white arrow). **F** DWI obtained from a 52-year-old man demonstrating high-intensity lesions in the right temporal cortex and the left striatum. The bilateral medial thalami also showed high intensity lesion (black arrows)

no family history of prion disease had the M232R substitution: one was previously reported, pathologically confirmed dementia with Lewy bodies [12], one was encephalitis, and one was not diagnosed yet, but was confirmed as not having CJD because his symptoms rather fluctuated. There remains the possibility that the M232R substitution is a rare polymorphism, not a causative point mutation [6], although the M232R substitution was not found among 100 healthy controls [4].

Discussion

In the present study, by reviewing the clinical and laboratory findings of 21 patients, we found that there were two distinct phenotypes in CJD232 in spite of the same genotype of PRNP, M232R, MM129, and GG219. Different phenotypes with the same pathogenic changes of PRNP are known in several types of genetic prion disease [14–21]. Fatal familial insomnia and gCJD with a common point mutation at codon 178 are well-known. However, the different phenotypes are regulated by a polymorphism at codon 129 [14, 15]. Similarly, a phenotypic variant of gCJD with a point mutation of glutamic acid to lysine at codon 200 (CJD200) is coupled with valine at codon 129 [19]. On the other hand, a thalamic variant of CJD200, which has the same polymorphism of MM129 as the vast majority of CJD200, has been reported [17, 21], although it is exceptional. In our results, 15 of the patients were the rapid-type, five were the slow-type. In CJD232, the slow-type, which has uncommon clinical features, is not exceptional and constitutes one of the major phenotypes because 25% of patients with CJD232 belong to the slow-type. Similarly, there are two different major phenotypes that are not influenced by the polymorphism of codon 129 and 219 in Gerstmann-Sträussler-Scherinker disease with a point mutation of proline to leucine at codon 102 of PRNP (GSS102), which is characterized by chronic cerebellar ataxia of long duration (several years or more) associated with neurological signs including dementia [21]. In GSS102, a sCJD-like variant of short duration (less than one year) has been reported [16]. In 27 patients with GSS102 recognized by the Creutzfeldt-Jakob Disease Surveillance

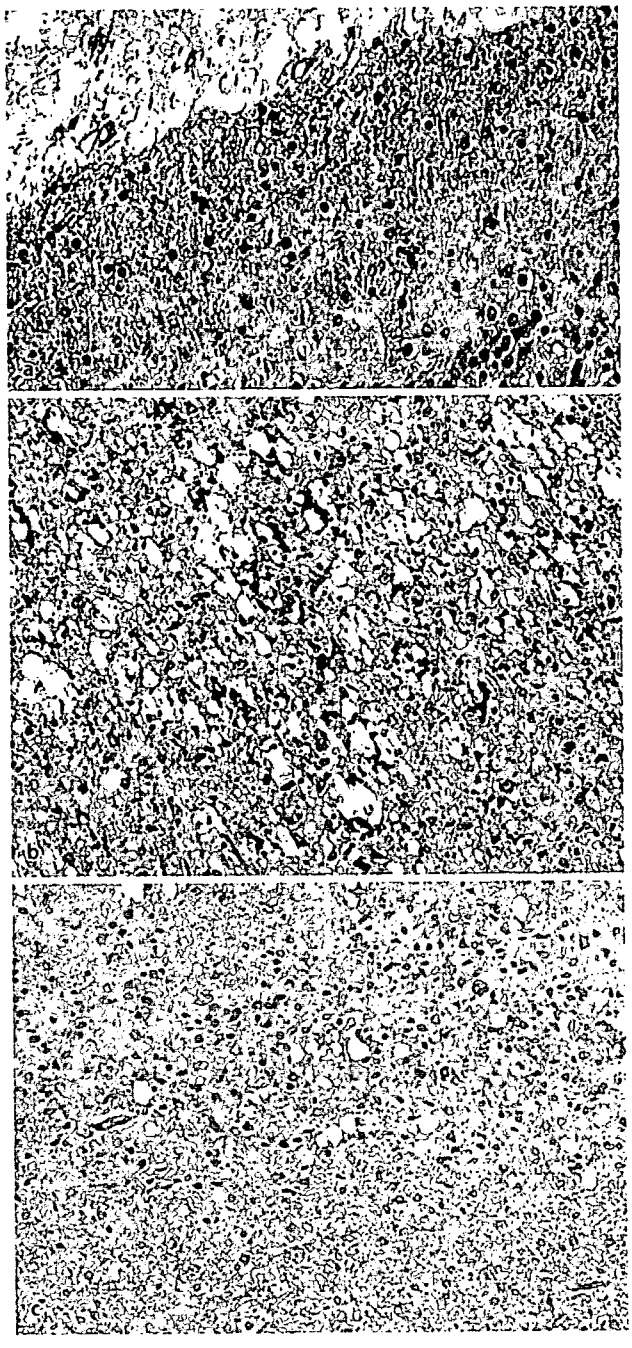

Fig. 4 Immunohistochemical staining of abnormal PrP using monoclonal antibody 3F4. **A** Anti-PrP immunostaining in a 67-year-old woman suffering from the rapid-type of CJD232 with an initial symptom of cerebellar ataxia. The molecular layer of the cerebellum shows a diffuse synaptic-type PrP deposit. Photographed at 200 times magnification. **B** Anti-PrP immunostaining in a 64-year-old woman suffering from the slow-type of CJD 232 with an initial symptom of dressing apraxia. This patient was previously reported by Satoh et al. (1997). The perivacuolar-type PrP deposit is predominantly demonstrated in the temporal cerebral cortex. Photographed at 50 times magnification. **C** Anti-PrP immunostaining in the same patient with Fig. 4B. The synaptic-type PrP deposit is demonstrated in the occipital cerebral cortex. Photographed at 50 times magnification

Committee, Japan until February 2006, five (18.5%) were this sCJD-like variant. It should be emphasized that CJD232 has two major different phenotypes with the completely same genotype of PRNP that is undoubtedly a major factor which influences the clinical phenotype [2, 22–24].

The gender and age at onset influence the disease progression [25]. However, there were no significant differences in the male to female ratio and age at onset between the two types in our series of CJD232. The molecular type of PrP^{Sc} is another factor that is closely associated with the clinical and pathological phenotypes of sCJD [26]. Unfortunately, the molecular type of PrP^{Sc} has not been sufficiently examined. One previously reported patient [27] in the rapid-type group had type 1 and one patient in the slow-type group had type 1 + 2. This difference may be a determinant of the clinical phenotypes of CJD232. More studies are needed to determine the relationship between the clinical phenotype and the molecular type of PrP^{Sc}. Immunohistochemical staining of PrP from four patients with the rapid-type revealed a diffuse synaptic-type deposit similar to that found in sCJD with MMI [28]. The synaptic-type PrP deposit may be an important pathological finding of the rapid-type. If so, we cannot differentiate the rapid-type of CJD232 from sCJD with MM1 based on the pathological findings. PrP immunohistochemical staining of three patients with the slow-type revealed that two had a perivacuolar-type and diffuse synaptic-type PrP deposits and one had only diffuse synaptic-type deposits. These pathological results suggest that the rapid-type might be a homogeneous group and the slow-type might not be. The number of studied patients in the two groups was too small to determine the pattern. If the PrP^{Sc} type 1 + 2 and the perivacuolar-type PrP deposits are key pathological features of the slow-type of CJD232, these may be related to the absence or late occurrence of myoclonus and PSWC on EEG, and the slower progression of the disease.

Diagnosing the rapid-type of CJD232 is not difficult because the patients start with progressing dementia, cerebellar ataxia, and visual problems, rapidly progress to akinetic mutism, demonstrate PSWC, are positive for 14-3-3 protein in the CSF immunoassay, and have characteristic MRI findings. These clinical features including the MRI findings are very similar to those of typical sCJD with MM1 [3] that accounts for the vast majority of sCJD. We can easily suspect CJD when we encounter such patients. Genetic examination of PRNP is necessary to differentiate the rapid-type of CJD232 from sCJD with MM1 [3] since a patient with CJD232 usually has no family history of prion disease or dementia, and differentiating CJD232 from sCJD with MM1 [3] is difficult when based on the clinical and laboratory features alone.

On the other hand, diagnosing the slow-type of

Table 1 Comparison of clinical and laboratory features between the rapid-type (R-type) and the slow-type (S-type) of CJD232

Clinical features	R-type (N = 15)	S-type (N = 5)	p
Age at onset (Year)	65.4 ± 5.2	59.0 ± 12.8	NS
Men: Women	8: 7	2: 3	NS
Family history	0/15 positive	0/5 positive	NS
Initial symptoms	7: progressive dementia 2: visual symptoms 2: cerebellar ataxia 2: involuntary movement 2: others	3: progressive dementia 1: psychiatric symptoms 1: dressing apraxia	
Myoclonus (Mo)[a]	2.4 ± 1.8	15.3 ± 12.3	< 0.005
Positive rate	14/14[b]	4/5*	NS
Akinetic mutism (Mo)[a]	3.1 ± 1.5	20.6 ± 4.4	< 0.001
Positive rate	15/15	5/5	NS
14-3-3 protein	8/8 positive	4/4 positive	NS
PSWC (Mo)[a]	2.8 ± 1.8	13	< 0.01
Positive rate	15/15	1/5**	< 0.01
MRI	8/9 positive	4/5 positive	NS
Codon 129	15: Met/Met	5: Met/Met	
Codon 219	14: Glu/Glu 1: Glu/Lys	5: Glu/Glu	
Autopsied cases	5/15	3/5	
PrP immunostaining	Synaptic: 4	Synaptic + Perivacuolar: 2 Synaptic: 1	
PrP type	Type 1: 1	Type 1 + 2: 1	

Values are means ± SD where applicable

[a] The duration until the appearance of myoclonus, akinetic mutism, and PSWC from the onset; [b] It was uncertain whether myoclonus had appeared or not in one patient

* Mean observation period was 14.8 ± 10.7 months; ** Mean observation period was 21.6 ± 12.8 months

R-type the rapid-type of CJD232; *S-type* the slow-type of CJD232; *PSWC* periodic sharp and wave complexes in EEG; *PRNP* prion protein gene; *Met/Met* methionine homozygosity; *Glu/Glu* glutamic acid homozygosity; *Glu/Lys* heterozygosity of glutamic acid and lysine; *NS* not significant

CJD232 is not easy because the patients initially manifest non-characteristic dementia or memory disturbance, or psychiatric symptoms as in other neurodegenerative disorders, progress relatively slowly, do not become akinetic and mute within a year, and do not demonstrate PSWC. When we diagnose the slow-type of CJD232, we cannot rely on PSWC, the presence of which is the most widely accepted diagnostic marker at the present time. In addition to the slow progression, the lack of a family history may cause this disease to be confused with other neurodegenerative disorders such as Alzheimer's disease, dementia with Lewy bodies, corticobasal degeneration, frontotemporal dementia, etc., especially in the early phase. MRI, especially DWI [11], is very useful to distinguish the slow-type of CJD232 from other neurodegenerative disorders, because the slow-type of CJD232 demonstrates CJD-related high-intensity lesions in DWI, whereas the above-mentioned neurodegenerative disorders do not demonstrate abnormal changes in signal intensities. There has been a report of suspected CJD patients who had M232R and in whom a final pathological diagnosis of dementia with Lewy bodies demonstrated no signal changes in DWI [12]. In our series of three patients with the slow-type examined by DWI, medial thalamic lesions were demonstrated. However, these lesions are not specific for the slow-type of CJD232, and we sometimes encounter them in sCJD [29]. The major differential diagnosis of the slow-type of CJD232 is sCJD with the MM2-cortical type [3], because the slow-type of CJD232 usually fulfills the previously advocated diagnostic criteria for sCJD with the MM2 cortical type [30]. It is hardly possible clinically to distinguish the slow-type of CJD232 from sCJD with the MM2 cortical type. However, the molecular type of PrP^{Sc} in one patient of the slow-type CJD232 was type 1 + 2, not type 2. The molecular types of PrP^{Sc} in each group may be different, although the presence of perivacuolar-type PrP deposits is also a finding of sCJD with the MM2-cortical type [3]. PRNP study is indispensable to distinguish between the two groups and molecular typing may be able to distinguish between them. We did not find any peculiar lesions of the slow-type such as a remarkable high intensity lesion in the cerebral cortex except for those in the medial occipital and cerebellar cortices which are characteristic of fCJD with a point mutation of valine to isoleucine at codon 180 (CJD180),

which is an unusual type of fCJD [13]. The degree of the abnormalities in MRI did not correlate with the disease severity. To diagnose the slow type of CJD232, recognizing the clinical phenotype that demonstrates uncommon clinical and laboratory features found in other neurodegenerative disorders with dementia and performing genetic examination of PRNP are important.

Other characteristics of CJD232 are that CJD232 patients have no family history of CJD or dementia in either type and are reported only in Japan. More than half of genetic prion disease patients with various PRNP mutations lack family histories and the lack of family histories is not restricted to CJD232 [1]. De novo mutations [31] and very low penetration [32] are considered as the reasons. Individual PRNP mutations also show variable geographical distributions [1]. The M232R substitution may influence the disease progression because the M232R substitution extended the incubation time in an experimental transmission study using humanized knock-in mice [33]. Three suspected patients with M232R substitution but with a final diagnosis of diseases other than CJD have been reported to the Creutzfeldt-Jakob Disease Surveillance Committee, Japan because they had the M232R substitution, not because they had clinical symptoms suspecting CJD. Therefore, we think that the prevalence of 6% in 50 non-CJD patients is not the same as that of the normal Japanese population. At least, it cannot be said that all patients having the M232R substitution demonstrate the symptoms of CJD232, and it does not seem to be supported that M232R substitution is a causative mutation. On the other hand, two probable CJD patients with M232R substitution in one family have been reported [6]. We cannot overlook these patients based on the fact that M232R substitution is very rare [4]. Whether M232R is really a causative mutation or only a rare polymorphism is another issue that needs to be resolved. We need more studies of CJD patients with M232R substitution, and especially the correlation between the pathological findings including the molecular type of PrP^{Sc} and immunohistochemical staining of PrP and the clinical findings should be clarified to determine whether it influences the disease progression. We need to study the morbidity of a population having the M232R substitution to determine whether it is a causative mutation or not.

□ **Acknowledgement** We thank Mr. Brent Bell for reading the manuscript. We also wish to thank all the doctors for their care of the patients. This study was based on the fruits of the Creutzfeldt-Jakob Disease Surveillance Committee, Japan and was supported in part by a grant from the Research Committee on Prion Disease and Slow Virus Infection, Ministry of Labor and Health, Japan. Yusei Shiga, Tetsuyuki Kitamoto, Shigetoshi Kuroda, Takeshi Sato, Yoshikazu Nakamura, Masahito Yamada, and Hidehiro Mizusawa are the members of the Creutzfeldt-Jakob Disease Surveillance Committee, Japan. The surveillance study of the Creutzfeldt-Jakob Disease Surveillance Committee, Japan was approved by the ethics committee of Kanazawa University.

References

1. Kovács GG, Puopolo M, Ladogana A, et al. (2005) Genetic prion disease: the EUROCJD experience. Hum Genet 118:166–174
2. Kovács GG, Trabattoni G, Heinfellner JA, Ironside JW, Knight RSG, Budka H (2002) Mutations of the prion protein gene: Phenotypic spectrum. J Neurol 249:1567–1582
3. Parchi P, Giese A, Capellari S, et al. (1999) Classification of sporadic Creutzfeldt-Jakob disease based on molecular and phenotypic analysis of 300 subjects. Ann Neurol 46:224–233
4. Kitamoto T, Ohta M, Doh-ura K, Hitoshi S, Terao Y, Tateishi J (1993) Novel missense variants of prion protein in Creutzfeldt-Jakob disease or Gerstmann-Sträussler Syndrome. Biochem Biophys Res Commun 191:709–714
5. Shimizu T, Tanaka K, Tanahashi N, Fukuuchi Y, Kitamoto T (1994) Creutzfeldt-Jakob disease with a point mutation at codon 232 of prion protein – A case report. Clin Neurol 34: 590–592
6. Hoque MZ, Kitamoto T, Furukawa H, et al. (1996) Mutation in the prion protein gene at codon 232 in Japanese patients with Creutzfeldt-Jakob disease: a clinicopathological, immunohistochemical and transmission study. Acta Neuropathol 92:441–446
7. Satoh A, Goto H, Satoh H, et al. (1997) A case of Creutzfeldt-Jakob disease with a point mutation at codon 232: Correlation of MRI and neurological findings. Neurology 49:1469–1470
8. Saito T, Isozumi K, Komatsumoto S, Nara M, Suzuki K, Doh-ura K (2000) A case of codon 232 mutation-induced Creutzfeldt-Jakob disease visualized by the MRI-FLAIR images with atypical clinical symptoms. Clin Neurol 40: 51–54
9. Tagawa A, Natsuno T, Suzuki M, Ono S, Shimizu N (2001) Creutzfeldt-Jakob disease with codon 232 point mutation and showing myoclonus and PSD in the early stage. A case report. Neurol Med 54:161–165
10. Hitoshi S, Nagura H, Yamanouchi H, Kitamoto T (1993) Double mutations at codon 180 and codon 232 of the PRNP gene in an apparently sporadic case of Creutzfeldt-Jakob disease. J Neurol Sci 120:208–212
11. Shiga Y, Miyazawa K, Sato S, et al. (2004) Diffusion-weighted MRI abnormalities as an early diagnostic marker for Creutzfeldt-Jakob disease. Neurology 63:443–449
12. Koide T, Ohtake H, Nakajima T, et al. (2002) A patient with dementia with Lewy bodies and codon 232 mutation of PRNP. Neurology 59:1619–1621
13. Jin K, Shiga Y, Shibuya S, et al. (2004) Clinical features of Creutzfeldt-Jakob disease with V180I mutation. Neurology 62:502–505
14. Goldfarb LG, Peterson RB, Tabaton M, et al. (1992) Fatal familial insomnia and familial Creutzfeldt-Jakob disease: disease phenotype determined by a DNA polymorphism. Science 258: 806–808

15. Monari L, Chen SG, Brown P, et al. (1994) Fatal familial insomnia and familial Creutzfeldt-Jakob disease: different prion proteins determined by a DNA polymorphism. Proc Natl Acad Sci 91:2839–2842
16. Barbanti P, Fabbrini G, Salvatore M, et al. (1996) Polymorphism at codon 129 or 219 of PRNP and clinical heterogeneity in a previously unreported family with Gerstmann-Sträussler-Scherinker disease (PrP-P102L mutation). Neurology 47:734–741
17. Chapman J, Arlazoroff A, Goldfarb LG, et al. (1996) Fatal insomnia in a case of familial Creutzfeldt-Jakob disease with the codon 200^{Lys} mutation. Neurology 46:758–761
18. Young K, Clark HB, Piccardo P, Dlouhy SR, Ghetti B (1997) Gerstmann-Sträussler-Scherinker disease with the PRNP P102L mutation and valine at codon 129. Molecular Brain Research 44:147–150
19. Hainfellner JA, Parchi P, Kitamoto T, Jarius C, Gambetti P, Budka H (1999) A novel phenotype in familial Creutzfeldt-Jakob disease: Prion protein gene E200K mutation coupled with valine at codon 129 and type 2 protease-resistant prion protein. Ann Neurol 45:812–816
20. Yamada M, Itoh Y, Inaba A, et al. (1999) An inherited prion disease with a PrP P105L mutation: Clinicopathologic and PrP heterogeneity. Neurology 53: 181–188
21. Teratuto AL, Piccardo P, Reich EG, et al. (2002) Insomnia associated with thalamic involvement in E200K Creutzfeldt-Jakob disease. Neurology 58:362–267
22. Doh-ura K, Tateishi J, Sasaki H, Kitamoto T, Sasaki Y (1989) Pro-leu change at position 102 of prion protein is the most common but not the sole mutation related to Gerstmann-Sträussler syndrome. Biochem Biophys Res Commun 163:974–979
23. Furukawa H, Kitamoto T, Tanaka Y, Tateishi J (1995) New variant prion protein in a Japanese family with Gerstmann-Sträussler-Scherinker syndrome. Brain Res Mol Brain Res 30:385–388
24. Shibuya S, Higuchi J, Shin RW, Tateishi J, Kitamoto T (1998) Codon 219 Lys allele of PRNP is not found in sporadic Creutzfeldt-Jakob disease. Ann Neurol 43:826–828
25. Pocchiari M, Puopolo M, Croes EA, et al. (2004) Predictors of survival in sporadic Creutzfeldt-Jakob disease and other human transmissible spongiform encephalopathies. Brain 127: 2348–2359
26. Hill AF, Joiner S, Wadsworth JD, et al. (2003) Molecular classification of sporadic Creutzfeldt-Jakob disease. Brain 126:1333–1346
27. Satoh K, Muramoto T, Tanaka T, et al. (2003) Association of an 11–12 kDa protease-resistant prion protein fragment with subtypes of dura graft-associated Creutzfeldt-Jakob disease and other prion diseases. J General Virol 84:2885–2893
28. Kitamoto T, Shin RW, Doh-ura K, et al. (1992) Abnormal isoform of prion proteins accumulates in the synaptic structures of the central nervous system in patients with Creutzfeldt-Jakob disease. Am J Pathol 140:1285–1294
29. Young GS, Geschwind MD, Fischbein NJ, et al. (2005) Diffusion-weighted and fluid-attenuated inversion recovery imaging in Creutzfeldt-Jakob disease: High sensitivity and specificity for diagnosis. Am J Neuroradiol 26: 1551–1562
30. Hamaguchi T, Kitamoto T, Sato T, et al. (2005) Clinical diagnosis of MM2-type sporadic Creutzfeldt-Jakob disease. Neurology 64:643–648
31. Dagvadorj A, Peterson RB, Lee HS, et al. (2003) Spontaneous mutations in the prion protein gene causing transmissible spongiform encephalopathy. Ann Neurol 52:355–359
32. Mitrova E, Belay GI (2002) Creutzfeldt-Jakob disease with E200K mutation in Slovakia: characterization and development. Acta Virol 46:31–39
33. Taguchi Y, Mohri S, Ironside JW, Muramoto T, Kitamoto T (2003) Humanized knock-in mice expressing chimeric prion protein showed varied susceptibility to different human prions. Am J Pathol 163:2585–2593

Journal of Neuroscience Research 85:2196–2206 (2007)

Impairment of Microglial Responses to Facial Nerve Axotomy in Cathepsin S–Deficient Mice

Hai Peng Hao,[1] Katsumi Doh-ura,[2] and Hiroshi Nakanishi[1]*

[1]Laboratory of Oral Aging Science, Faculty of Dental Sciences, Kyushu University, Fukuoka, Japan
[2]Department of Prion Research, Tohoku University, Sendai, Japan

Cathepsin S (CS) is a lysosomal/endosomal cysteine protease especially expressed in cells of a mononuclear lineage including microglia. To better understand the role of CS in microglia, we investigated microglial responses after a facial nerve axotomy in CS-deficient (CS−/−) and wild-type mice. Microglia in both groups accumulated in the facial motor nucleus following axotomy. However, the mean number of microglia in CS−/− mice on the axotomized side was significantly smaller than that in wild-type mice. Microglia were found to adhere to injured motoneurons in wild-type mice, whereas microglia abutted on injured motoneurons without spreading on their surface in CS−/− mice. At the same time, the axotomy-induced down-regulation of tenasin-R, an antiadhesive perineuronal net for microglia, was partially abrogated in CS−/− mice. Primary cultured microglia prepared from CS−/− mice showed that CS deficiency caused significant suppression of migration and transmigration of microglia. In CS−/− mice, impaired recruitments of circulating monocytes and T lymphocytes and reduced expression of the class II major compatibility complex on the axotomized side were observed. Interestingly, cathepsin B, a typical lysosomal cysteine protease, was markedly expressed on the axotomized side in CS−/− but not in wild-type microglia. Finally, we compared axotomy-induced neuronal death in the two groups and found that the percentage of motoneurons that survived in CS−/− mice was significantly smaller than that in wild-type mice. The present study strongly suggests that CS plays a role in the migration and activation of microglia to protect facial motoneurons against axotomy-induced injury.

Key words: cathepsin S–deficient mice; facial nerve axotomy; microglia; cathepsin B; transmigration; motoneuron survival

Cathepsin S (CS) is a member of the lysosomal cysteine protease family, which is preferentially expressed in cells of mononuclear-phagocytic origin including microglia (Petanceska et al., 1996). In response to lipopolysaccharide (LPS), a substantial increase in the activity of CS secreted from both macrophages and microglia is observed (Petanceska et al., 1996). CS retains its proteolytic activity even after prolonged exposure to a neutral pH (Bromme et al., 1989, 1993). CS has been reported to degrade several extracellular matrix (ECM) molecules including fibrillar collagen, elasin, laminin, fibronectin, and heparan sulfate proteoglycans at a neutral pH (Liuzzo et al., 1999). CS-deficient (CS−/−) monocytic cells showed impaired subendothelial basement membrane transmigration (Sukhova et al., 2003). Furthermore, CS plays a pivotal role in antigen presentation because this enzyme is an essential requirement for invariant chain processing in antigen-presenting cells including dendritic cells and microglia (Nakagawa et al., 1999; Shi et al., 1999; Nishioku et al., 2002) without affecting expression of the class II major compatibility complex (MHC II). The cell type–specific localization and enzymatic nature of CS both contrast sharply with other types of lysosomal cysteine proteases including cathepsin B (CB). CB is expressed in almost all cell types and is also secreted from microglia as the heavy chain form in addition to the proform on stimulation with LPS (Ryan et al., 1995). However, it is well known that CB is irreversibly inactivated at a neutral pH. In addition to playing a role in intracellular proteolysis, CS secreted by microglia and monocytic cells may also play a role in extracellular proteolysis among different types of lysosomal cysteine proteases. We may therefore speculate that CS plays a specific role in the reactions of microglia and monocytic cells including migration, adhesion, transmigration, and antigen presentation (Nakanishi, 2003).

It is well known that microglia exhibit a series of reactions after facial nerve axotomy (Ravich et al., 1999; Moran and Graeber, 2004). Following axotomy, micro-

Contract grant sponsor: Ministry of Education, Science and Culture, Japan; Contract grant numbers: 17390495, 17659578, and 17659578 (all to H.N.).

*Correspondence to: Hiroshi Nakanishi, PhD, Laboratory of Oral Aging Science, Faculty of Dental Sciences, Kyushu University, Fukuoka 812-8582, Japan. E-mail: nakan@dent.kyushu-u.ac.jp

Received 1 November 2006; Revised 4 January 2007 and 24 February 2007; Accepted 8 March 2007

Published online 30 May 2007 in Wiley InterScience (www.interscience.wiley.com). DOI: 10.1002/jnr.21357

glia are rapidly activated and then are transformed into a deramified form; thereafter, they proliferate, adhere to injured motoneurons, and spread on their surfaces. Monocytic cells recruited to the brain parenchyma through the cerebral vasculature and the leptomeninges also adhere to injured motoneurons (Priller et al., 2001; Bechmann et al., 2005). Although the precise pathological significance of the perineuronal satellite position of microglia remains unclear, the adhesion of microglia to injured motoneurons may be essential for neuronal survival, thus leading to axonal regeneration. Activated microglia may displace synaptic input, a phenomenon known as synaptic stripping (Blinzinger and Kreutzberg, 1968). The tight adhesion of microglia could enhance uptake of diffusible molecules leaked from injured motoneurons and trans-synaptic uptake of their breakdown products as well as of pathogens (Ravich et al., 1999; Kalla et al., 2001). On the other hand, microglia express MHC II and costimulatory factors (Streit et al., 1989) and interact with T lymphocytes recruited to the axotomized facial motor nucleus (Ravich et al., 1998). Therefore, microglia may also play a pivotal role in immune surveillance as an antigen-presenting cells in the axotomized facial motor nucleus. Following a facial nerve axotomy, there was marked up-regulation in microglia of CS and cystatin C (CysC), the latter an endogenous inhibitor for cysteine proteases (Miyake et al., 1996; Uwabe et al., 1997). Up-regulation of CS may be closely associated with microglial responses to a facial nerve axotomy because ECM degradation is required for the rapid migration, adhesion, and transmigration of microglia and monocytic cells. Moreover, CS is essential for antigen presentation by microglia (Nishioku et al., 2002). However, no report has previously elucidated the precise function of CS in microglial reactions to a facial nerve axotomy.

In the present study, we examined the effects of CS deficiency on microglial reactions to a facial nerve axotomy and facial motoneuron survival. We found that CS deficiency markedly impaired cellular responses of microglia to a facial nerve axotomy, thereby promoting axotomy-induced facial motoneuron death.

MATERIALS AND METHODS

Animals

Heterozygous mice (CS+/−) mice on a DBA background were provided by Dr. William H. Brissette (Central Research Division, Pfizer Inc., Groton, CT; Nakagawa et al., 1999) and maintained under specific pathogen-free conditions at Kyushu University Faculty of Dentistry. Selection of CS−/− mice from littermates obtained by heterozygous coupling was performed by template genomic DNA isolated from tail biopsies examined to detect the neomycin cassette by neoexon 6– and exon 5–specific PCR with primers of cs6-1 (5′-TACCCGCTTCCATTGCTCAG-3′), cs6-2 (5′-TCTTTCAGGGCATCTTCGTC-3′), cs5-1 (5′-GGTTCTTGTGGTGCCTGTTG-3′), and cs5-2 (5′-GTGGCTTTGTAGGGATGGA-3′).

Surgical Procedures

All operations were performed under anesthesia with pentobarbital (40 mg/kg intraperitoneally, i.p.). The right facial nerves of 6-week-old CS−/− and wild-type mice were transected approximately 1 mm at the stylomastoid foramen. Failure of a mouse to move the whiskers on the right side of the face following recovery from anesthesia was considered verification of the success of the axotomy.

Immunohistochemistry

Detailed indirect fluorescent immunohistochemistry has been previously described (Nakanishi et al., 2001; Shimizu et al., 2005). Briefly, 2, 4, 7, 14, 30, and 50 days after axotomy, the specimens were obtained from CS−/− and wild-type mice (n = 4 each), which were anesthetized with sodium pentobarbital (40 mg/kg, i.p.) and killed by intracardiac perfusion with isotonic saline, followed by a chilled fixative consisting of 4% paraformaldehyde (PFA) in 0.2M phosphate-buffered saline (pH 7.4). After perfusion, the brain was removed, further fixed by immersion in the same fixative overnight at 4°C, and then immersed in 20% sucrose (pH 7.4) for 24 hr at 4°C. Floating parasagittal sections (30 μm thick) of the brain stem were prepared by a cryostat (CM1850 Leica, Nusloch, Germany) and stained with rabbit polyclonal anti-ionized calcium-binding adaptor molecule 1 (Iba1) antibody (1:500; Wako Pure Chemical Industries, Ltd., Osaka, Japan), OX6 (1:100; Serotec, Oxford, UK), mouse monoclonal anti–tenascin R (TNR) antibody (1:100; R&D Systems Inc., Minneapolis, MN), or rabbit polyclonal anti–choline acetyltransferase (ChAT, 1:500; Chemicon International) for 3 days at 4°C. After washing with phosphate-buffered saline (PBS), the sections were stained with biotinylated antirabbit, antimouse, or antigoat IgG (Vector Laboratories, Burlingame, CA) overnight. After washing with PBS, the sections were stained with ABC reagent (Vector Laboratories, Burlingame, CA) or Alexa 488 0.5% streptavidin (Molecular Probes, Eugene, OR). The sections that reacted with ABC reagent were developed with diaminobenzidine, dehydrated in alcohol and xylene, and then mounted. The sections that reacted with Alexa 488 streptavidin were mounted with Vectashield antifading medium (Vector Laboratories).

For double staining, floating parasagittal sections (30 μm thick) of the brain stem were incubated with goat polyclonal anti-CS antibody (1:300; Santa Cruz Biotechnology, Inc., Santa Cruz, CA), rabbit polyclonal anti-CB (1:200; Upstate, Lake Placid, NY), anti-ChAT (1:500), rabbit polyclonal anti-CysC (1:300; Upstate), or mouse monoclonal anti-CD3 (1:500; BD Biosciences, Bedford, MA) antibody for 3 days at 4°C. After washing with PBS, the sections were treated with 0.5% antirabbit or antigoat IgG conjugated with Cy3 (Jackson ImmunoResearch Laboratories, Inc., West Grove, PA) for 2 hr at room temperature. They were then further treated with anti-Iba1 antibody (1:500) or F4/80 (1:50; Serotec, Oxford, UK) for 3 days at 4°C. After washing with PBS, the sections were treated with 0.5% antirabbit IgG or antimouse IgG conjugated with Alexa 488 (Molecular Probes, Eugene, OR) for 2 hr at room temperature. The sections incubated with anti-ChAT antibody were also treated with 0.5% anti-

rabbit IgG conjugated with Alexa 488 (Molecular Probes) for 2 hr at room temperature. The sections were treated with mouse monoclonal anti-GFAP antibody (Sigma, St. Louis, MO) for 3 days at 4°C and then were further incubated with 0.5% antimouse IgG conjugated with Cy3 (Jackson Immunoresearch Laboratories). The sections were mounted in the Vectashield antifading medium (Vector Laboratories, Burlingame, CA) and examined by a confocal laser scanning microscope (CLSM; LSM510META, Carl Zeiss, Jena, Germany).

Evaluation of Microglial Morphology

To quantitatively describe the differences in microglial morphology between CS−/− and wild-type mice after axotomy, we adopted a transformation index (TI), which was calculated by the equation, [perimeter of cell (μM)]^2/4π [cell area (μm^2)] (Fujita et al., 1996). Five sections (30 μm thick) stained with anti-Iba1 antibody were randomly selected from each of the CS−/− and wild-type mice (n = 3 each). Images of individual sections, photographed with a conventional CCD camera with a 20× objective (numerical aperture = 0.75), were analyzed with an image analyzer to determine their perimeters and areas. The TI was calculated for the axotomized and control sides of the CS−/− and wild-type mice 2, 4, and 7 days after axotomy.

Electrophoresis and Immunoblotting

The supernatant fractions of the facial nuclei were prepared from CS−/− (n = 3) and wild-type (n = 3) mice 7 days after axotomy, in which the mice were anesthetized with sodium pentobarbital (40 mg/kg, i.p.) and killed by intracardiac perfusion with isotonic saline. Each homogenate was electrophoresed in 7%–12% sodium dodecyl sulfate (SDS)–polyacrylamide gels. Proteins on SDS gels were transferred electrophoretically to nitrocellulose membranes. The protein transfers were blocked in 5% skim milk for 1 hr at room temperature under gentle agitation. The blots were then incubated with anti-CS (1:1,000), anti-CB (1:1,000), anti-CysC (1:1,000), anti-TNR (1:500), or antiactin (1:1,000, Santa Cruz Biotechnology, Santa Cruz, Santa Cruz, CA) antibodies overnight at 4°C under gentle agitation. After washing, the blots were incubated with 0.02% horseradish peroxidase (HRP)–labeled donkey antirabbit or antimouse IgG (Amersham). Subsequently, the membrane-bound, HRP-labeled antibodies were detected by an enhanced chemiluminescence detection system (ECL kit, Amersham) with an image analyzer LAS-1000 (Fuji Photo Film, Tokyo, Japan). The protein bands were then scanned and analyzed densitometrically.

mRNA Extraction and Reverse Transcriptase (RT)-PCR

mRNA was prepared from the facial nuclei from CS−/− (n = 3) and wild-type (n = 3) mice 7 days after axotomy, and then the mice were anesthetized with sodium pentobarbital (40 mg/kg, i.p.) using a QuickPrep micro mRNA purification kit (Amersham Oharmacia Biotech, England, UK), and the first cDNA was synthesized using SuperScript II (Invitrogen, Carlsbad, CA). For PCR, the cDNA was amplified by Tag DNA polymerase (Invitrogen). Reverse transcription was performed at 60°C for 15 min in 0.5 mg of mRNA. PCR amplification was performed in the DNA amplifier cycle (Techne Duxford, UK) after an initial cycle at 94°C for 2 min for 40 cycles of 1 min at 94°C and 1.5 min at 60°C. The RT-PCR products were run on 2% agarose gel and stained with ethidium bromide. Glyceroldehydes-3-phosphate dehydrogenase (GAPDH)–specific primers were used as a control with 1 mL of template cDNA. Primers for CS were 5′-GACATTGCCTGACACTGTGG-3′ and 5′-CATGTTCACATTGCCCGTA-3′, primers for CB were 5′-CTCTGGAGCATGGAGCTTCT-3′ and 5′-ATGCCACAGTGGTTTTCTCC-3′, primers for CysC were 5′-AGCGAGTACAAC-AAGGGCAG-3′ and 5′-CAAGAAGAGTGAAGCCAGGG-3′, and primers for GAPDH were 5′-TCCACCACCCTGTTGCTGTA-3′ and 5′-ACCACAGTCCATGCCATCAC-3′.

Microglial Culture

Microglia were isolated from mixed primary cell cultures from whole-brain samples of 3-day-old CS−/− and wild-type mice according to methods described previously (Nishioku et al., 2002). Eagle's minimal essential medium (MEM) containing 10% fetal calf serum, penicillin G (40 U/mL), and streptomycin (50 mg/mL) was used for culture medium. After 10–14 days in culture, floating cells and weakly attached cells in the mixed glial cell layer were isolated by shaking of the flask. The resulting cell suspension was transferred to a petri dish (Falcon 1001, Lincoln Park, NJ) and allowed to adhere at 37°C. Unattached cells were removed after 30 min, and microglia were isolated as strongly adhering cells. The microglia were more than 96% pure, as determined by the immunostaining of Iba1.

Cell Proliferation Assay

Cell viability was measured 24 hr after treatment with macrophage colony-stimulating factor (M-CSF, R&D Systems Inc., Minneapolis, MN) or granulocyte macrophage colony-stimulating factor (GM-CSF, Genzyme, Cambridge, MA) by WST-8 conversion to water-soluble formazan by mitochondrial dehydrogenase (Cell Counting Kit-8, Dojindo, Kumamoto, Japan). Briefly, WST-8 was added to the culture medium of primary cultured microglia prepared from CS−/− and wild-type mice growing in serum-free medium and incubated at 37°C for 4 hr. The supernatant was transferred to 96-well dishes and then was quantitated using a plate reader at 450 nm.

Cell Migration Assay

Cell migration of microglia was assessed using the Boyden chamber. Polycarbonate filters with pores of 3 μM precoated with fibronectin (Becton Dickison Labware, Bedford, MA) were used. Five hundred microliters of microglial cell suspension in serum-free MEM containing 0.3% bovine serum albumin prepared from CS−/− and wild-type mice was plated on cell inserts at a cell density of 10^5. All inserts were dipped into lower wells contained 750 μL of serum-free MEM containing 100 μM ATP as a chemical attractant. The plates were incubated at 37°C in a 10% CO_2 atmosphere for 6 and 24 hr. Cells remaining on the upper surface of the

membrane were removed by wiping, and migrated cells were fixed with 4% PFA and subjected to Diff-Quik stain (Sysmex Corp., Kobe, Japan). Microglia that migrated to the lower surface of the membrane were manually counted in eight randomly chosen fields under a microscope with a 20× objective. Each assay was performed in triplicate.

Cell Transmigration Assay

Cell transmigration of microglia was assessed using a Matrigel chamber. Polycarbonate filters with pores of 8 μM precoated with Matrigel basement membrane matrix (BD Biosciences) were used. Five hundred microliters of microglial cell suspension in serum-free MEM containing 0.3% bovine serum albumin prepared from CS−/− and wild-type mice was plated on cell inserts at a cell density of 2×10^5. All inserts were dipped into lower wells contained 750 μL of serum-free MEM containing 100 μM ATP as a chemical attractant. In some experiments using primary culture microglia prepared from wild-type mice, benzyloxycarbonyl-Phe-Leu-α-keto-β-aldehyde (Z-FL-COCHO; Calbiochem, San Diego, CA), a specific inhibitor of CS, was added to serum-free MEM. Plates were incubated at 37°C in 10% CO_2 atmosphere for 24 hr. Cells remaining on the upper surface of the membrane were removed by wiping and the transmigrated cells were fixed with 4% PFA and subjected to Diff-Quik stain (Sysmex Corp.). The number of microglia that transmigrated to the lower surface of the membrane was manually counted in eight randomly chosen fields under a microscope with a 20× objective. Each assay was performed in triplicate.

Intrasplenic Injection of 6-Carboxylfluorescein Diacetate (CFDA)

CS−/− and wild-type mice (n = 3 each) were anesthetized with sodium pentobarbital (40 mg/kg, i.p.). A 0.5 cm incision was made on the left lateral abdomen. After preparing the surface of the spleen, 100 μL of a solution containing 2% of the long-lasting fluorescent tracker CFDA (Molecular Probes) in 0.1M PB was slowly injected. Twenty-four hours after the intrasplenic injection of CFDA, the right-side facial nerves were axotomized.

Quantitative Analysis of Facial Motoneurons

The optical dissector method using CLSM images (Jinno et al., 1998; Shimizu et al., 2005) was used to measure the numerical density of facial motoneurons. Five 30-μm-thick serial sections of a facial motor nucleus stained with anti-ChAT antibody were prepared from CS−/− and wild-type mice (n = 3 each) that had been subjected to facial nerve axotomy 4, 7, 30, and 50 days earlier. Images of individual sections were taken as a stack at 1-μm step size along the z direction with a 20× objective by a CLSM (LSM510MET). Data were transferred to a Power Mac G4 computer (Apple) and then analyzed using NIH Image software (version 1.62). Antibodies from the surface sufficiently permeated the full thickness of both CS−/− and wild-type mice brain sections. The number of ChAT-immunoreactive cells in each of five serial sections of a facial motor nucleus was summed. The data were averaged for each animal and then for each group. The calculated numerical profile densities of the groups were compared using the Student t test.

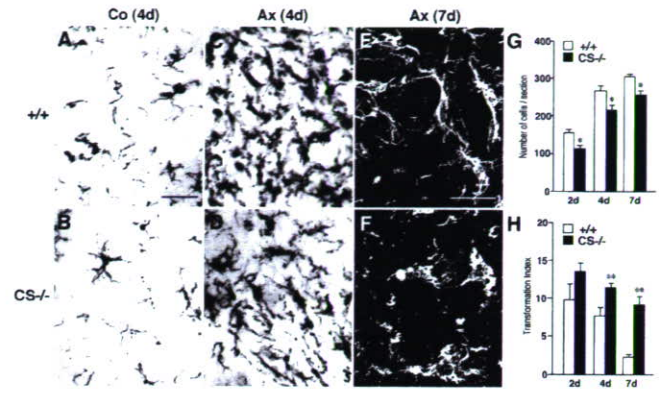

Fig. 1. Microglial responses following facial nerve axotomy in CS−/− and wild-type mice. **A:** Iba1-stained microglia in facial motor nuclei on control side (Co) of wild-type mice 4 days after axotomy. Scale bar = 50 μm. **B:** Iba1-stained microglia in facial motor nuclei on Co side of CS−/− mice 4 days after axotomy. **C:** Iba1-stained microglia in facial motor nuclei on axotomized side (Ax) of wild-type mice 4 days after axotomy. **D:** Iba1-stained microglia in facial motor nuclei on Ax side of CS−/− mice 4 days after axotomy. **E:** High-resolution CLSM images of Iba1-stained microglia on the axotomized side of facial motor nuclei of wild-type mice 7 days after axotomy. Scale bar = 25 μm. **F:** High-resolution CLSM images of Iba1-stained microglia on the axotomized side of facial motor nuclei of CS−/− mice 7 days after axotomy. Each section was taken as a stack at 1-μm step size along the z direction with a 100× objective by a CLSM. **G:** Number of microglia accumulated in axotomized facial motor nuclei of wild-type and CS−/− mice (open and solid columns, respectively) 2, 4, and 7 days after axotomy. Each column and bar represents the mean ± SD of three experiments (*significant difference at $P < 0.05$). **H:** TI of microglia accumulated in the axotomized facial motor nuclei of wild-type and CS−/− mice (open and solid columns, respectively) 2, 4, and 7 days after axotomy. TI was calculated by the equation [perimeter of cell (μM)]^2 /4π [cell area (μm^2)].

Statistical Analysis

Data are expressed as means ± SDs. The statistical analyses were performed using the Student t test.

RESULTS

Alterations of Microglial Responses to Facial Nerve Axotomy in CS−/− Mice

No obvious abnormality in CS−/− mice compared to wild-type mice was noticed. We first focused on the microglial responses to the facial nerve axotomy. Following axotomy, microglia on the axotomized side of mice in both groups showed activated cell morphology characterized by a large cell body with thick processes. On the other hand, microglia on the control side maintained a normal ramified morphology (Fig. 1A,B). Four days after axotomy, there was a marked difference between the two groups in the morphology of microglia on the axotomized side. In wild-type mice, microglia had relatively small

cell bodies with thin processes (Fig. 1C). In contrast, in CS−/− mice most microglia still had rather large cell bodies with short processes (Fig. 1D). These morphological differences in microglia became more prominent 7 days after axotomy. CLSM images clearly showed that microglia spread on the surfaces of injured motoneurons, forming a thin continuum rimlike structure, in the wild-type mice (Fig. 1E). In CS−/− mice, most microglia still had rather large cell bodies with short processes and abutted injured motoneurons without spreading on their surface (Fig. 1F).

We further quantitated the number and morphological transformation of microglia on the axotomized side of the facial motor nuclei of both groups. As shown in Figure 1G, the mean number of microglia that had accumulated on the axotomized side of the facial motor nuclei of CS−/− mice was significantly smaller than that of wild-type mice. The morphological transformation of microglia after axotomy was also quantitated as a TI using the equation [perimeter of cell (μM)]^2/4π [cell area (μm^2)]. The mean TI of CS−/− mice was significantly larger than that of wild-type mice 4 days after axotomy (Fig. 1H).

Reduced TNR Down-Regulation in Facial Motor Nuclei of CS−/− Mice following Axotomy

Next, we tried to determine why the CS−/− microglia failed to spread on the surfaces of facial motoneurons after axotomy. It has been reported that TNR that presents in the perineuronal net of motoneurons acts as antiadhesive for activated microglia (Angelov et al., 1998). Furthermore, expression of TNR was markedly down-regulated after axotomy. Therefore, it is tempting to speculate that insufficient down-regulation of TNR in CS−/− mice may prevent microglia from spreading onto the surfaces of axotomized facial motoneurons. To determine if this were true, we examined the level of TNR in the facial motor nuclei of CS−/− and wild-type mice after axotomy. In both groups, the total amount of TNR significantly decreased on the axotomized side (Fig. 2A). However, there was a greater decrease in the amount of TNR in the CS−/− mice than in the wild-type mice. This was substantiated with immunostaining with anti-TNR antibody (Fig. 2B). Although the immunoreactivity for TNR diffusely spread throughout a facial motor nucleus, the most intense immunoreactivity was found on the surface of cell somata of motoneurons in both groups. Seven days after axotomy, there was a marked reduction in the immunoreactivity for TNR on the axotomized side of the facial motor nuclei of wild-type mice. In contrast, only a moderate reduction in immunoreactivity for TNR was found in the CS−/− mice.

Effects of CS Deficiency on ATP-Induced Migration/Transmigration and GM-CSF-Induced Proliferation of Primary Cultured Microglia

Rapid accumulation of microglia occurred in the facial nuclei after axotomy mainly because of the proliferation and migration of microglia as a result of cellular activation (Ravich et al., 1999; Moran and Graeber, 2004). There is increasing evidence that in addition to the contributions made by proliferation and migration, recruitment of monocytic cells through the cerebral vasculature and the leptomeninges also adds to the increased number of microglia on the axotomized side of the facial motor nucleus (Priller et al., 2001; Bechmann et al., 2005). Thus, we next compared the proliferative, migratory, and proliferative abilities of primary cultured microglia prepared from CS−/− and wild-type mice because there was a significant reduction in the number of microglia on the axotomized side of the facial motor nuclei of CS−/− mice.

M-CSF is a major mitogen for microglia in the axotomized facial nucleus (Raivichet al., 1994). Furthermore, an experiment involving GM-CSF binding in axotomized facial nuclei showed GM-CSF to be a plausible mitogen (Ravich et al., 1991). We thus used both M-SCF and GM-CSF as mitogens to examine the effect of CS deficiency on cell-proliferating ability. As shown in Figure 3A, there was no significant difference between the two groups in the cell-proliferating ability of microglia after stimulation with either M-CSF or GM-CSF. We next conducted ATP-induced cell migration assay using a Boyden chamber. The wild-type and CS−/− microglia that migrated to the opposite side of the fibronectin-coated membrane after treatment with ATP were counted. As shown in Figure 3B, the mean number of migrated CS−/− microglia 24 hr after treatment with

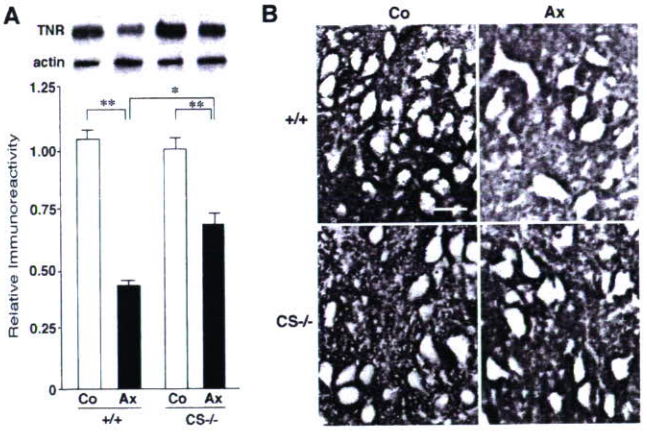

Fig. 2. Reduction in axotomy-induced down-regulation of TNR in facial motor nuclei of CS−/− mice 7 days after axotomy. **A:** Immunoblot analyses of TNR levels on the control (Co) and axotomized (Ax) sides (open and solid columns, respectively) of facial motor nuclei of CS−/− and wild-type mice. Mean relative immunoreactivity of TNR band was determined using expression of actin as an internal control. Each column and bar represents the mean ± SD of three experiments (**significant difference at $P < 0.01$). **B:** Immunohistochemical staining of TNR on Co and Ax sides of facial motor nuclei of CS−/− and wild-type mice. A marked reduction in the immunoreactivity for TNR was observed in axotomized facial motor nuclei of wild-type mice but not in CS−/− mice. Scale bar = 75 μm.

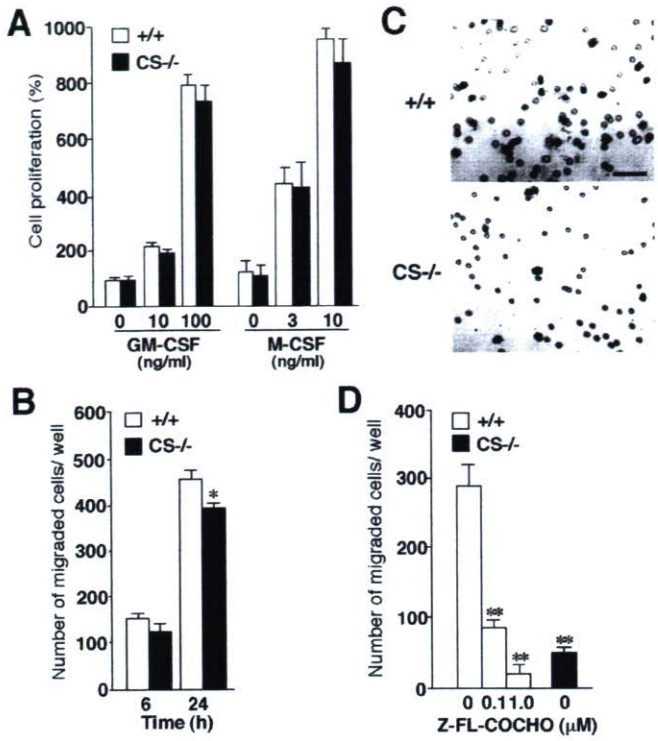

Fig. 3. Effects of CS deficiency on proliferation, migration, and transmigration of primary cultured microglia. **A:** Mean survival ratio of CS−/− and wild-type microglia 24 hr after treatment with M-CSF or GM-CSF. Each column and bar represents the mean ± SD of three experiments. **B:** ATP-induced migration of primary cultured microglia prepared from CS−/− and wild-type mice detected by the Boyden chamber. Mean number of CS−/− and wild-type microglia that migrated to the opposite side of a fibronectin-coated membrane, assessed by a Boyden chamber 6 and 24 hr after treatment with ATP (100 μM). Each column and bar represents the mean ± SD of three experiments (*significantly different from the wild-type microglia at $P < 0.05$). **C, D:** ATP-induced transmigration of primary cultured microglia prepared from CS−/− and wild-type mice, detected by a Matrigel invasion chamber. **C:** CS−/− and wild-type microglia that transmigrated to the opposite side of the Matrigel basement membrane matrix. Scale bar = 85 μm. **D:** Mean number of CS−/− and wild-type microglia as well as wild-type microglia treated with Z-FL-COCHO that transmigrated to opposite side of the Matrigel basement membrane matrix 24 hr after treatment with ATP (100 μM). Each column and bar represents the mean ± SD of three experiments (**significantly different from the wild-type control at $P < 0.01$).

ATP (100 μM) was slightly but significantly smaller than that of migrated wild-type microglia. We further conducted an ATP-induced cell transmigration assay using a Matrigel invasion chamber. The mean number of CS−/− microglia transmigrated through the Matrigel basement membrane matrix 24 hr after treatment with ATP (100 μM) was significantly lower than that of wild-type microglia (Fig. 2C,D). Furthermore, a specific inhibitor of CS, Z-FL-COCHO, significantly inhibited the transmigration of wild-type microglia through the Matrigel basement membrane matrix in a dose-dependent manner (Fig. 3D).

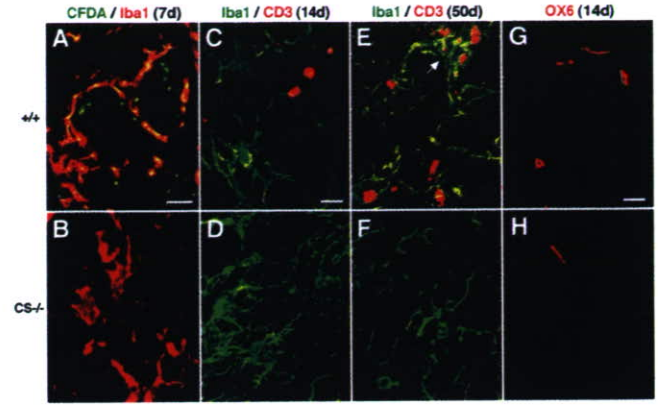

Fig. 4. Impairment of axotomy-induced recruitment of CFDA-labeled splenocytes and T lymphocytes in the facial motor nuclei of CS−/− mice. **A:** Immunofluorescent CLSM image of facial motor nuclei of wild-type mice 7 days after axotomy showing that the CFDA-labeled cells (green) are visible on the axotomized side. Scale bar = 35 μ. **B:** Immunofluorescent CLSM image of facial motor nuclei of CS−/− mice 7 days after axotomy showing that the CFDA-labeled cells (green) are not visible on the axotomized side. The CFDA-labeled cells corresponded well with microglia (red), which spread on the surface of injured facial motoneurons. **C:** CLSM image of infiltrated CD3-positive T lymphocytes (red) and Iba1-positive microglia (green) in facial motor nuclei of wild-type mice 14 days after axotomy. Scale bar = 40 μm. **D:** CLSM image of infiltrated CD3-positive T lymphocytes (red) and Iba1-positive microglia (green) in facial motor nuclei of CS−/− mice 14 days after axotomy. **E:** CLSM image of infiltrated CD3-positive T lymphocytes (red) and Iba1-positive microglia (green) in facial motor nuclei of wild-type mice 50 days after axotomy. Scale bar = 40 μm. **F:** CLSM image of infiltrated CD3-positive T lymphocytes (red) and Iba1-positive microglia (green) in facial motor nuclei of CS−/− mice 50 days after axotomy. **G:** CLSM images of immunoreactivity for MHC II-positive cells in facial motor nuclei of wild-type mice 14 days after axotomy. Scale bar = 30 μm. **H:** CLSM images of immunoreactivity for MHC II-positive cells in facial motor nuclei of CS−/− mice 14 days after axotomy.

Z-FL-COCHO did not have a significant cytotoxic effect on primary cultured microglia in the concentration range used in this study (data not shown).

Impaired Recruitment of Monocytic Cells and T Lymphocytes and Reduced MHC II Expression in Facial Motor Nuclei of CS−/− Mice after Axotomy

To further evaluate the effects of CS deficiency on cell transmigration, we examined the recruitment of monocytic cells and T lymphocytes into facial motor nuclei after axotomy. Seven days after axotomy, CFDA-fluorescent granules were detected on the axotomized side of the facial motor nuclei of intrasplenic CFDA-injected wild-type mice. These CFDA fluorescent granules were found to localize in 13% ± 3% of the Iba1-positive microglia (Fig. 4A). In contrast, we could not detect any CFDA fluorescent granules in the facial motor nuclei of CFDA-injected CS−/− mice (Fig. 4B). These obser-